mathematics

MDPI

Article

Low-Carbon Scheduling Optimization for Flexible Job Shop Production with a Time-of-Use Pricing Strategy and a Photovoltaic Microgrid

Qi Lu [1,2], Chenxu Wei [1,*], Zirong Guo [1], Xiangang Cao [1], Chao Zhang [3,4] and Guanghui Zhou [3,4]

[1] School of Mechanical Engineering, Xi'an University of Science and Technology, Xi'an 710054, China; luqi@xust.edu.cn (Q.L.); 23205224074@stu.xust.edu.cn (Z.G.)
[2] Shaanxi Key Laboratory of Mine Electromechanical Equipment Intelligent Detection and Control, Xi'an University of Science and Technology, Xi'an 710054, China
[3] School of Mechanical Engineering, Xi'an Jiaotong University, Xi'an 710049, China; ghzhou@xjtu.edu.cn (G.Z.)
[4] State Key Laboratory for Manufacturing Systems Engineering, Xi'an Jiaotong University, Xi'an 710054, China
* Correspondence: 23205224127@stu.xust.edu.cn

Abstract

To achieve "carbon peak and carbon neutrality" in manufacturing, this paper tackles high energy consumption in flexible job shop production by developing a low-carbon scheduling optimization model with time-of-use electricity pricing, incorporating a photovoltaic microgrid. The model minimizes makespan, carbon emissions, and costs, considering photovoltaic power uncertainty, energy storage dynamics, and time-of-use pricing. To address coupled scheduling and energy management challenges, a three-stage bilevel collaborative optimization framework is proposed, enhancing the Multi-Objective Particle Swarm Optimization (MOPSO) algorithm to develop a Collaborative MOPSO (CMOPSO). The improved algorithm features a four-layer encoding mechanism with energy factors, chaotic mapping for better global search, and adaptive mutation for population diversity. Validation using the Brandimarte benchmark demonstrates the algorithm's robustness. Specifically, comparative experiments reveal that the proposed strategy significantly outperforms the traditional scheduling mode. While maintaining a similar makespan, the proposed method reduces production costs by 44.3% and carbon emissions by 29%. Simulations confirm that the method effectively shifts tasks to low-price periods and leverages photovoltaic energy during peak hours, supporting the manufacturing industry's green transition.

Keywords: flexible job shop; photovoltaic microgrid; time-of-use pricing; multi-objective optimization; low-carbon scheduling

MSC: 90C29

Check for updates

Academic Editors: Antonio Di Crescenzo, Andrea Scozzari and Ziyan Zhao

Received: 24 December 2025
Revised: 30 January 2026
Accepted: 6 February 2026
Published: 8 February 2026

Copyright: © 2026 by the authors. Licensee MDPI, Basel, Switzerland. This article is an open access article distributed under the terms and conditions of the Creative Commons Attribution (CC BY) license.

1. Introduction

As a pillar of the national economy, the manufacturing sector accounts for 70% of China's industrial carbon emissions [1] and ranks among the world's highest in terms of energy consumption and carbon output [2], thus facing multiple pressures from energy security and environmental protection perspectives, as well as international competition. With the intensification of global climate change and the introduction of "carbon neutrality" and "carbon peak" goals, the green and low-carbon transformation of manufacturing is not only a manifestation of social responsibility, but also an inevitable choice for enhancing

core competitiveness. Traditional production scheduling prioritizes efficiency and cost, but against the backdrop of increasingly complex energy structures and pricing, it urgently requires integration of environmental considerations. Energy consumption is highly concentrated in production workshops. Optimized scheduling—through scientifically planning workpiece processing sequences, resource selection, and equipment start/stop times—can achieve significant energy savings without additional hardware investment. Research indicates that idle machine energy waste can account for over 40% of total energy consumption [3]. Optimized scheduling reduces waiting times and minimizes equipment idling and start-ups, thereby effectively lowering energy consumption and carbon emissions [4], making it a low-cost, high-efficiency approach to workshop energy conservation.

Although optimized scheduling has proven effective for energy conservation, traditional methods primarily rely on single-grid power supply models. They fail to fully leverage new opportunities presented by increasingly widespread photovoltaic microgrids and market-driven time-of-use electricity pricing. As a clean, renewable energy source, photovoltaic microgrids introduce new challenges to workshop scheduling due to the fluctuating and unpredictable nature of their power generation [5]. Concurrently, time-of-use pricing provides enterprises with an economic incentive to reduce operational costs by adjusting production sequences through varying electricity rates across different time periods [6].

To address these challenges, scholars worldwide have conducted extensive research on the Green Flexible Job Shop Scheduling Problem (GFJSP), renewable energy optimization, and time-of-use pricing.

For the Green Flexible Job Shop Scheduling Problem, researchers have developed a diverse range of optimization methods, spanning from exact algorithms to meta-heuristics. Zhao et al. [7] provided a systematic synthesis of the applications of Iterated Greedy Algorithms within the domain of flow-shop scheduling. Their work not only establishes a standardized algorithmic framework and offers a rigorous comparative analysis of various destruction and construction strategies, but also presents an in-depth classification of complex scheduling scenarios, such as distributed and no-wait configurations. Furthermore, as green scheduling typically involves conflicting objectives and inherent uncertainties, specialized evolutionary approaches have emerged. Zhang et al. [8] proposed a decomposition-based multi-objective evolutionary algorithm with clustering and hierarchical estimation (MOEA/D-CH) for fuzzy flexible job shop scheduling, leveraging clustering techniques to manage weight vectors and enhance population diversity. Building upon these advancements, Zhao et al. [9] recently introduced a dynamic quadratic decomposition strategy. Unlike traditional linear aggregation, this nonlinear approach dynamically balances exploitation and exploration, demonstrating superior efficacy in addressing high-dimensional multi-objective optimization problems. Luan et al. [10] proposed an augmented NSGA-II to optimize the completion time, machine load, total dragging time, and total energy consumption in GFJSP. Liu et al. [11] specifically designed a machine restart strategy that balances energy consumption and lifespan, proving that a well-conceived restart mechanism can effectively harmonize low carbon emissions with long-term system reliability. Meng et al. [12] constructed six novel MILP models to optimize the total energy consumption for the problem of considering machine switching machines. Wei et al. [13] first constructed an energy estimation model to compute the energy consumption of the machine under different operating states for the problem of considering speed scaling strategy and then designed a multi-objective optimization model to minimize the completion time and total energy consumption. Luo et al. [14] considered the machine failure problem and designed a knowledge-driven two-stage modelling algorithm to optimize the completion time and total energy consumption. Du et al. [15] considered the preparation time and

designed a weighted reinforcement learning-based approach to optimize the completion time and the total energy consumption, where the total energy consumption was further modeled by taking into account the machine's setup. Lv et al. [16] proposed a rescheduling algorithm to optimize the completion time and total energy consumption in the framework of a heuristic algorithm for dynamic events in the production process. However, existing studies still have some limitations regarding green scheduling modeling. While many scholars have considered resource constraints, dynamic events, machine starts and stops, and other production influences on the basis of the green flexible job shop scheduling problem, most of the literature still considers energy consumption and carbon emissions to be a single green indicator and does not consider the diversification of the energy supply structure. Especially in the current context of rapid development of renewable energy, traditional green scheduling research is mainly based on a single-grid power supply model, ignoring the impact of distributed renewable energy, energy storage systems, and other emerging energy technologies on scheduling strategies. Thus, the adaptability of research results to practical applications can be improved.

However, optimizing production scheduling in isolation is no longer sufficient to meet the demands of modern intelligent manufacturing. Current research trends are shifting toward integrated optimization of coupled subsystems, such as coordination between production and logistics or the energy supply. Zhao et al. [17] investigated an integrated system encompassing production and multi-mobile robot transportation. Their findings confirm that holistic modeling of interdependent systems—specifically by synchronizing logistical tasks with production processes—yields significantly superior performance compared to decoupled optimization strategies.

With the rapid development of distributed energy technologies and the "dual carbon" goal, the introduction of renewable energy sources such as photovoltaic (PV) power generation into manufacturing plants to reduce external grid dependence and carbon emissions has become a new research hotspot. As a kind of distributed energy system integrating PV power generation, energy storage systems, and intelligent control technology, PV microgrids have great potential to be applied in the manufacturing industry, but related research is still in the initial stage. Chen et al. [18] chose the manufacturing industry as the target of their study and investigated the environmental and economic impacts of the integrated energy system in various optimization scenarios; the results showed that PV power generation has better performance from the perspective of carbon emission reduction. Chakraborty et al. [19] proposed a coordinated frequency control strategy for PV microgrids as a solution for demand-side management by targeting thermostatic devices consisting of industrial loads for demand-side management, realizing the promotion of optimal demand-side management through frequency regulation. Huang et al. [20] developed an intelligent demand-corresponding plan for multi-energy industrial microgrids with an industrial process represented by the discrete manufacturing production model, the uncertainty of PV power generation, and the operating cost of Battery Energy Storage Systems (BESSs) as a challenge, formulated the problem as a scenario-based stochastic nonconvex mixed-integer nonlinear programming, and proposed a hybrid optimization algorithm incorporating evolutionary algorithms and branch-bounding algorithms, which efficiently reduces the operating cost of manufacturing production and releases pressure on the main grid. Zhang et al. [21] considered the uncertainty of future power market prices and PV generation and proposed a regret-based risk-averse stochastic production task and energy management model for industrial microgrids, which was applied to a battery manufacturing plant to analyze the impact of the total target production task and wind control parameters on the cost. Burmeister et al. [22] combined dynamic energy tariffs, energy storage systems, and renewable energy sources for an energy-aware dis-

patch methodology from uncertain dynamic markets, proposed a two-level energy-aware scheduling method based on a modular non-dominated sorting genetic algorithm, and set the scenario in the context of a green flexible scheduling shop to show the potential energy saving costs and carbon emissions. In summary, the existing literature has verified the technical feasibility and economic viability of introducing PV energy into factories and has carried out preliminary explorations at the level of industrial parks and workshops, but the research on in-depth integration and application in the workshop is relatively weak. In particular, optimization of coupled PV microgrids and flexible job shop scheduling has not yet been fully investigated.

The time-sharing tariff mechanism, as an important part of power market-oriented reform, guides users to optimize their electricity consumption behavior by setting differentiated tariffs for different time periods and realizes peak shaving and valley filling, as well as the supply-demand balance of the power system. For manufacturing enterprises, the time-sharing tariff strategy provides an opportunity to reduce operating costs by adjusting the production schedule, which also provides a new entry point and driving force for the optimization of green scheduling in the workshop. Deng et al. [23] proposed a price for optimizing power prices based on time-sharing tariffs to reduce the cost of the grid, which provides theoretical support for the design of a time-sharing tariff mechanism. Yu et al. [24] investigated the complex multilevel task network scheduling and cooperative optimization of electric power supply in the context of time-sharing tariffs, integrating distributed energy sources, and proposed a hybrid algorithm, which was verified to have excellent performance in terms of reducing energy consumption and costs. Jia et al. [25] took the effect of variable energy prices on energy cost into account and constructed a multi-objective optimization model with cost, carbon emission, and customer satisfaction as the objectives; the experimental results showed that the method can significantly reduce carbon emissions, improve customer satisfaction, and enhance the competitiveness and green production image of the enterprise. Park et al. [26] explored the impacts of time-of-use tariffs and planned downtime with flexible job shop scheduling and proposed an integer linear programming model; the results showed that energy costs can be significantly reduced while maintaining maximum productivity. Shen et al. [27] investigated how to minimize the total energy cost under a time-sharing tariff scheme within the framework of the flexible job shop scheduling problem and proposed an iterative forbidden search algorithm for the general problem, verifying the scheme's potential benefits in terms of total energy cost reduction. Although studies confirm that time-sharing tariffs optimize energy allocation, enhance microgrid stability, and reduce manufacturing costs and carbon emissions, current research focuses on shop floor energy allocation, overlooking clean photovoltaic renewable energy integration. Notably, there has been insufficient systematic study on combining time-sharing tariffs, PV microgrids, and flexible shop scheduling, particularly regarding PV power generation timing, tariff period matching, and energy storage systems' role in peak shaving and valley filling, revealing clear research gaps.

In summary, although significant progress has been made in algorithmic efficiency and multi-system integration, a critical theoretical gap remains regarding the deep coupling mechanism between stochastic renewable energy supply and flexible production loads. A fundamental challenge lies in the mathematical heterogeneity of the two domains: flexible job shop scheduling is a typical discrete combinatorial optimization problem involving integer variables, whereas microgrid energy management involves a continuous power flow dynamic. Most existing approaches treat energy supply as a static constraint or optimize objectives in isolation, failing to mathematically bridge the gap between discrete task allocation and continuous energy dispatch. Consequently, simply applying traditional strategies is insufficient. There is an urgent need to establish a bi-level collabo-

rative optimization framework that can simultaneously coordinate these heterogeneous variables to achieve a mathematically rigorous synergistic reduction in energy costs and carbon emissions.

To bridge this gap, this paper develops a multi-objective collaborative optimization model coupling FJSP with PV microgrids using TOU pricing. To solve this complex model, a three-stage bilevel collaborative framework is designed, and an improved Collaborative Multi-Objective Particle Swarm Optimization (CMOPSO) algorithm is proposed. The main contributions and novelties of this study are as follows:

1. A Coupled Low-Carbon Scheduling Model: Unlike traditional methods that treat energy supply as a static constraint, this study establishes a dynamic coupling model between the FJSP and PV microgrids. By incorporating TOU pricing and PV uncertainty, the model realizes dual optimization of "energy supply" and 'production load.
2. A Three-Stage Bilevel Collaborative Framework: A novel hierarchical solution framework is proposed to decompose the complex coupled problem. It consists of preliminary scheduling, PV availability analysis, and integrated optimization, effectively bridging the timescale difference between production tasks and energy management.
3. An Improved CMOPSO Algorithm: To solve this high-dimensional NP-hard problem, the CMOPSO algorithm is enhanced with a four-layer encoding mechanism (incorporating energy source decisions), logistic chaotic mapping for global search initialization, and an adaptive mutation strategy to maintain population diversity and avoid local optima.

2. Optimization Model for Low-Carbon Dispatch of Flexible Job Shop Production and Photovoltaic Microgrids

Taking the flexible job shop production process as the research object and considering the dynamic energy supply of photovoltaic microgrids comprehensively, studying how to optimize the two-layer scheduling strategy of time and energy in order to simultaneously reduce the energy consumption of production, improve the processing efficiency, and reduce the cost of production is a core challenge in the field of smart manufacturing and sustainable development. Flexible shop floor scheduling is characterized by flexible task allocation and efficient resource utilization, but its high energy consumption problem limits the development of low-carbon manufacturing. Photovoltaic microgrids can significantly reduce carbon emissions through providing a renewable energy supply, but the stochastic and fluctuating nature of power generation puts higher requirements on real-time scheduling. To solve this problem, this paper constructs a multi-objective optimization model coupling flexible workshop production and photovoltaic microgrids. The model includes the following sub-models: (1) a job shop scheduling model for optimizing task allocation and minimizing maximum completion time; and (2) a PV microgrid model for dynamically managing energy supply and storage. The modeling process of each model is described below.

2.1. Low-Carbon Photovoltaic Flexible Shop Floor Scheduling Model

The photovoltaic flexible job shop scheduling problem aims to achieve synergistic optimization of productivity, energy consumption, and cost by optimizing production task allocation and energy supply strategies. The Flexible Job Shop Scheduling Problem (FJSP) involves assigning multiple tasks on multiple machines; each task contains several processes, and each process can be processed by any one of a set of available machines. Compared to traditional job shop scheduling, FJSP has higher complexity due to process

flexibility and machine selection diversity, and optimization usually includes minimizing finish-time energy consumption.

The assumptions of the problem are as follows. (1) At the initial moment (t = 0), all the workpieces are in the state of pending processing, all the machines are in the idle state, and all the workpieces can start processing immediately. (2) The processes for the same workpiece have a strict order of priority, while different workpieces have the same priority, with no priority constraints. (3) At any time, each machine can only process one process, and once the process starts, it cannot be interrupted. (4) Photovoltaic power generation is based on the known daily power generation curve, without considering weather effects. (5) The initial capacity of the energy storage system is known, and the charging and discharging efficiency is fixed. (6) The grid electricity price follows the time-of-day tariff mechanism, and the tariff function is fixed during the dispatch cycle. (7) Machine failures, random delays in workpiece addition, or real-time fluctuations in PV power generation are not taken into account; the electrical devices (machines) are assumed to operate under fixed working conditions. The specific machining parameters (e.g., cutting speed, feed rate) and the rated power of the equipment are constant values.

Table 1 shows a symbolic representation of the model.

Table 1. Symbolic representation of scheduling problem models.

Symbol	Definition
i,g	Workpiece index, i,g = 1, 2, . . ., n
j,h	Process index
k	Machine index, k = 1, 2, . . ., m
O_{ij},O_{gh}	Process j of workpiece i, process h of workpiece g
T_{ijk}	Machining time on machine k for the jth pass of workpiece i
T_k^I	Total standby idle time for machine k
S_{ij}	Processing start time for O_{ij}
C_{ij}	Processing end time for O_{ij}
S_{ijk}	Process start time on machine k
C_{ijk}	End machining time of the process on machine k
C_i	Completion time of workpiece i
$\tau_{ijk}(t)$	The effective processing duration of operation O_{ij} within the t-th time period
P_k^M	Average processing power of machine k
P_k^I	Standby power of machine k
E_{proc}	Total processing energy consumption
E_{idle}	Total standby energy consumption
E_{com}	Total idle energy consumption
C	Total carbon emissions
$C_{\max}$	Maximum completion time
t	Time slot index, $t \in \{1, 2, \ldots, T\}$
Δt	Duration of each time slot, 1 h
f_{grid}	Grid carbon emission factor
f_{pv}	PV carbon emission factor
L	A sufficiently large positive number

In this model, we introduce the following binary decision variables to represent the production scheduling and resource allocation choices:

$$X_{ij} = \begin{cases} 1, \text{ Select the jth process of workpiece i} \\ 0, \text{ otherwise} \end{cases}$$

$$Y_{ijk} = \begin{cases} 1, \text{ Process } O_{ij} \text{ immediately after machining in machine k} \\ 0, \text{ otherwise} \end{cases}$$

where X_{ij} and Y_{ijk} are decision variables.

2.1.1. Integrated Carbon Emissions Model

The carbon emissions considered in PV flexible job shop scheduling are mainly composed of two carbon emission modules: the grid-supplied carbon emission module and the PV-supplied carbon emission module. The carbon emissions from both are closely related to the energy consumption generated by job shop production activities, which mainly includes machine tool energy consumption and public energy consumption, and machine tool energy consumption mainly includes machining energy consumption and idle waiting energy consumption.

(1) Machining energy consumption refers to the energy consumed by the machine tool in the machining state, and the total machining energy consumption is

$$E_{\text{proc}} = \sum_{i=1}^{n} \sum_{j=1}^{l_i} \sum_{k=1}^{m} (X_{ij} T_{ijk} P_k^M) \tag{1}$$

(2) Idle waiting energy consumption is the energy consumed by a machine tool that appears to be idle because it has not arrived or there is no production run taking place on the machine, and the idle waiting energy consumption of machine k is

$$E_{idle} = \sum_{k=1}^{m} \left(T_k^{\text{I}} P_k^{\text{I}} \right) \tag{2}$$

(3) Public energy consumption refers to the energy consumption of public facilities in the workshop, which is the energy that must be consumed in order to maintain normal operation of the workshop, and is the sum of energy consumption for lighting, ventilation, air conditioning, etc. The public power is a fixed value of P_0, and its total energy consumption is

$$E_{com} = P_0 C_{\max} \tag{3}$$

Therefore, the expression for the total energy consumption of the workshop is

$$E = E_{proc} + E_{idle} + E_{com} \tag{4}$$

(4) The total energy consumption of the workshop is calculated as E. However, calculating carbon emissions accurately requires addressing the mismatch between the time granularity of scheduling and energy pricing. The scheduling variables (e.g., start time S_{ijk}) are continuous, while the grid's electricity prices are discrete, typically changing on an hourly basis.

To bridge this gap, we introduce a time discretization mapping mechanism. Let the entire scheduling horizon be divided into T discrete time slots, indexed by $t = 1, 2, \ldots, T$, with each slot having a duration of Δt (e.g., $\Delta t = 1$ h). For a specific operation O_{ij} processed on machine k, the continuous processing interval $\left[S_{ijk}, C_{ijk} \right]$ is mapped onto the discrete time slots. The effective processing duration $\tau_{ijk}(t)$ of this operation within the t-th time slot is calculated as the intersection of the two time intervals:

$$\tau_{ijk}(t) = \max(0, \min(C_{ijk}, t \cdot \Delta t) - \max(S_{ijk}, (t-1) \cdot \Delta t)) \tag{5}$$

Based on this mapping, the total energy consumption in the t-th time slot, denoted as $E_{total}(t)$, can be accurately derived by summing the power consumption of all operations and idle states active during that slot. Consequently, the total carbon emission C is formulated by summing the emissions over all discrete time slots, considering the time-varying grid emission factor $f_{grid}(t)$:

$$C = f_{\text{grid}} \cdot \sum_{t=1}^{T} E_{\text{grid}}(t) + f_{PV} \cdot \sum_{t=1}^{T} E_{PV}(t) \tag{6}$$

where $E_{grid}(t)$ and $E_{PV}(t)$ represent the energy supplied by the grid and the photovoltaic system in time slot t, respectively, subject to the power balance constraints described in Section 2.3.

In this study, the carbon emission factors are treated as constant parameters based on regional standards [28]: the grid emission factor f_{grid} is set to 0.641 $kgCO_2/kWh$, and the PV emission factor f_{PV} is 0.055 $kgCO_2/kWh$.

2.1.2. Photovoltaic Microgrid Model

The photovoltaic microgrid model aims to provide efficient and economical energy support for flexible shop floor scheduling by dynamically managing the renewable energy supply and the energy storage system, while reducing total system energy consumption and carbon emissions. The PV microgrid consists of a PV power generation system, an energy storage system, and an external power grid. In this study, the photovoltaic panels are installed on the roof of the workshop to form a distributed generation system, ensuring direct power supply to the production line and minimizing transmission losses. Its core task is to optimize the energy distribution strategy according to the real-time power demand of the shop floor production, maximizing utilization of PV power generation and minimizing dependence on the external power grid.

(1) Photovoltaic power model

In microgrid optimal scheduling, the power of PV cells must be predicted. The output power model of PV cell is shown below:

$$P_{\text{pv}} = R_{\text{pv}} q_{\text{pv}} \frac{I_{\text{T}}}{I_{\text{STC}}} [1 + \alpha_{\text{p}}(T_{\text{c}} - T_{\text{stc}})] \tag{7}$$

where P_{pv} is the output active power of the PV cell; R_{pv} is the output power of the PV cell under standard test conditions; q_{pv} is the derating coefficient of the PV cell, which is usually 0.8; I_T is the actual intensity of solar radiation; I_{STC} is the intensity of solar radiation under standard test conditions; α_{P} is the temperature coefficient of the PV panel; T_{c} is the temperature of the PV cell during the current time step; T_{c} is the temperature of the PV cell during the current time step; and T_{stc} is the PV cell temperature under standard test conditions.

Considering that photovoltaic power generation has instability, in order to simulate the energy output characteristics of photovoltaic power generation, a solar photovoltaic power station in a province in the northwest region of China was selected as an example [29]. As shown in Figure 1, the red dots represent the selected actual measured data samples, while the curve represents the fitted power generation trend based on the normal distribution model, illustrating a typical all-day power generation output.

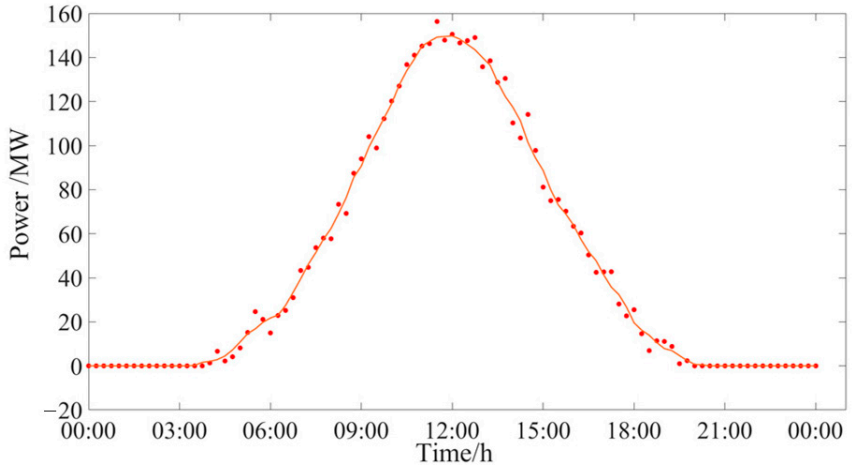


Figure 1. Photovoltaic power output curve.

Based on the photovoltaic power generation curve shown above, the energy generated by photovoltaic power generation p_t is

$$p_t = \int_{t_0}^{t_1} Pv(t)dt \tag{8}$$

where t_0 denotes the beginning moment of a cycle, t_1 denotes the end moment of a cycle, and $P_v(t)$ denotes the amount of energy that the PV can produce at moment t.

Since PV power generation is approximately normally distributed throughout the day, it can be described by the probability density function of the normal distribution as

$$Pv(t) = W \times \exp\left(-\frac{(t-12)^2}{8}\right),\ t \in [0,24] \tag{9}$$

where W represents the peak value of PV power generation in a day.

(2) Battery model

Batteries are a kind of energy storage equipment. In the case of renewable energy, if a power supply cannot meet the load needs, batteries will release their stored energy to provide users with a stable power supply, to ensure safe and stable operation of the system.

$$SOC(t) = \begin{cases} SOC(t-1) + \frac{1}{\eta^-} P_{\text{bess}}(t), P_{\text{bess}}(t) \leqslant 0 \\ SOC(t-1) + \eta^+ P_{\text{bess}}(t), P_{\text{bess}}(t) > 0 \end{cases} \tag{10}$$

where $SOC(t)$ is the remaining capacity of the battery at time t; $P_{\text{bess}}(t)$ is the charging and discharging power of the battery at time t; positive means charging and negative means discharging; and η^+ and η^- are the charging and discharging efficiencies, respectively.

(3) Time-sharing tariff model

Time-sharing tariffs are the core tool of the electricity market pricing mechanism. Constructing a time-sharing tariff needs to take into account user demand, system cost changes, and other factors. According to China's time-sharing tariff policy, the tariff will be divided into three phases: peak time (10:00–12:00, 17:00–22:00), usual time (8:00–10:00, 12:00–17:00), and valley time (22:00–8:00 the next day). The time-of-day tariff model [30] is shown in Table 2.

Table 2. Time-of-day tariff model.

Type of Tariff	Electricity Price (Yuan/kW·h)	Time Slot
Valley	0.394	0:00–8:00, 22:00–0:00
Flat	0.707	8:00–10:00, 12:00–17:00
Peak	1.020	10:00–12:00, 17:00–22:00

2.2. Objective Function

We combined the GFJSP and PV problems to minimize completion time, carbon emissions, and cost. To do this, we established a mixed integer linear programming mathematical model, which minimizes the completion time objective function as follows:

$$\min C_{\max} \tag{11}$$

where $C_{\max}$ is the maximum completion time, which will change according to different scheduling schemes.

According to the carbon emission calculation method in Section 2.1.1, the carbon emission objective function is constructed as follows:

$$\min C \tag{12}$$

Based on the time-of-use tariff model, the following cost objective function is constructed:

$$\min W = \sum_{t=1}^{T} E_{proc} \times f(t) \tag{13}$$

where W is the cost incurred by the workshop in using electricity while carrying out production activities, and $f(t)$ is the time-sharing tariff function.

In summary, the multi-objective function for low-carbon scheduling of PV flexible shop scheduling is as follows:

$$\min F(x) = \begin{cases} f_1(X) = C_{\max} \\ f_2(X) = C(X) = \sum\limits_{t=1}^{T} \sum\limits_{k=1}^{k0} E_{grid} \times fgrid^N + \sum\limits_{i=1}^{i0} \sum\limits_{l=1}^{l0} Epv \times {f_{pv}}^N \\ f_3(X) = W(X) = \sum\limits_{t=1}^{T} E_{proc} \times f(t) \end{cases} \tag{14}$$

2.3. Constraints

In the actual process of production activities, PV microgrids need to consider the balance of the power supply and the output of the energy storage equipment, while the production process needs to consider the constraints on the processing of workpieces and machines.

2.3.1. Power Balance Constraints

The grid power supply, as the main source of energy supply for the workshop, usually has more stable output characteristics. Photovoltaics, as an auxiliary energy source, constitutes the normal operation of the workshop, in which power balance constraints need to be considered:

$$E_{\text{total}}(t) = \sum_{i=1}^{n} \sum_{j=1}^{l_i} \sum_{k=1}^{m} \left(P^{\text{proc}} \cdot \tau_{ijk}(t) \cdot X_{ij} \right) + E_{\text{idle}}(t) \tag{15}$$

$$E_{\text{grid}}(t) = \max(0, E_{\text{total}}(t) - P_{PV}(t) \cdot \Delta t - P_{\text{bess}}(t) \cdot \Delta t) \tag{16}$$

where $P_{PV}(t)$ is the power supplied by the PV, $E_{grid}(t)$ is the energy supplied by the grid, and $P_{bess}(t)$ is the power supplied by the batteries. The profile of $E_{total}(t)$ is dynamically determined by the decision variables S_{ij} and X_{ijk}, thereby establishing intrinsic mathematical coupling between the energy constraints (Equations (15)–(17)) and the scheduling domain (Equations (18)–(23)).

2.3.2. Energy Storage Device Constraints

The battery serves as a back-up power source for the shop, allowing for charging when there is sufficient PV energy and discharging when there is a shortage of PV energy, with the following constraints:

$$\begin{cases} P_{bess}^{min}(t) \leqslant P_{bess}(t) \leqslant P_{bess}^{max}(t) \\ SOC^{min}(t) \leqslant SOC(t) \leqslant SOC^{max}(t) \end{cases} \tag{17}$$

where $P_{bess}^{min}(t)$ and $P_{bess}^{max}(t)$ are the upper and lower limits, respectively, of the energy storage state output, whose values are positive for the power input and negative for the power output; and $SOC^{max}(t)$ and $SOC^{min}(t)$ are the upper and lower limits, respectively, of the energy storage capacity at the moment t.

2.3.3. Flexible Job Shop Constraints

The flexible job shop needs to consider mobilization of workpieces and machines during production activities, with the following constraints:

$$\sum_{k=1}^{m} x_{ijk} = 1, \ \forall i, j \tag{18}$$

$$S_{ij} + T_{ijk} X_{ijk} \leqslant C_{ij} \tag{19}$$

$$C_{ij} \leqslant C_i \tag{20}$$

$$C_{ij} \leqslant S_{i(j+1)} \tag{21}$$

$$S_{ijk} + T_{ijk} - L(1 - Y_{ijk}) \leqslant S_{ghk} \tag{22}$$

$$S_{ij} \geq 0, \ S_{ijk} \geq 0, \ T_{ijk} \geq 0 \tag{23}$$

Equation (18) specifies that a particular process can only be processed on one machine; Equation (19) indicates the time constraints of the process; Equation (20) ensures that the completion time of the process should not exceed the completion time of the corresponding workpiece; Equation (21) specifies that the various processes in the workpiece should follow the established sequence of processing; Equation (22) indicates that each machine can only be start a process after completion of the previous process and before beginning the next process (that is, only one process can be processed at a time); and Equation (23) indicates that the value of the parameter variable is non-negative.

3. Problem Solving Based on a CMOPSO Algorithm

Particle Swarm Optimization [31] (PSO) was proposed by Kennedy and Eberhart et al. in 1995, which guides the evolution of particle swarms to the global optimum by simulating the social cooperation and individual competition behaviors of flocks of birds and schools of fish, according to the currently searched optimal solutions. The multi-objective particle swarm algorithm is extended based on the classical particle swarm optimization algorithm, using an external population archive (Archive) to store all the current non-dominated solutions. Individuals in the external archive are considered elite individuals, controlling the direction of population evolution through the elite individuals, aiming at searching

for a set of non-dominated solutions in the solution space and guiding the population to approximate the real Pareto front, as well as using the particles in the external archive as an approximation of the Pareto optimal solution obtained at the end of the algorithm run.

3.1. Problem-Solving Framework

In this study, a three-stage feedback optimization framework is proposed to effectively solve the problem of shop floor scheduling and PV microgrid integration. The overall framework diagram shown in Figure 2 consists of three phases.

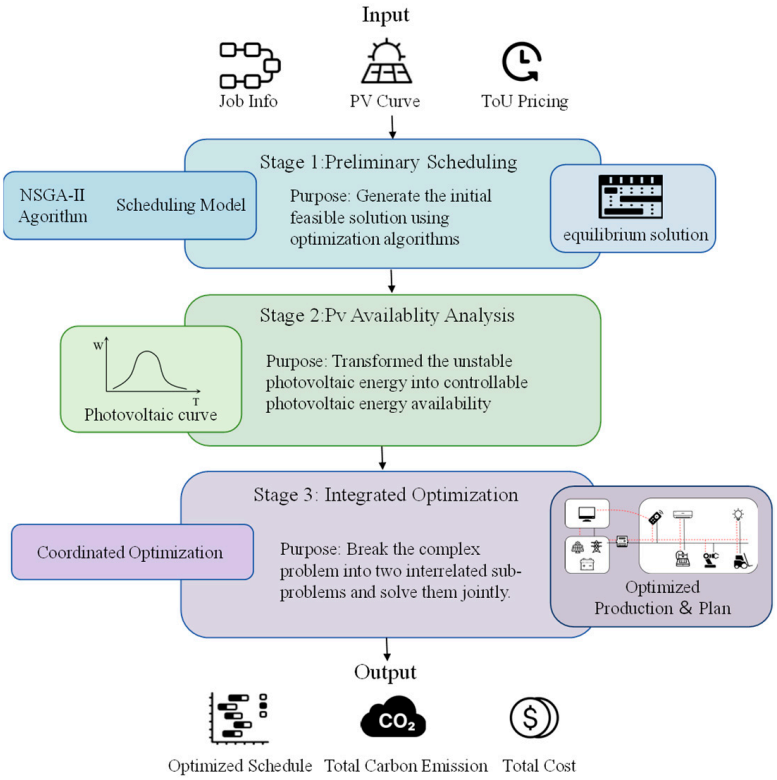


Figure 2. Three-stage problem solving framework.

3.1.1. Initial Carbon-Aware Scheduling

The problem of coupling job shop scheduling and PV microgrids requires simultaneous consideration of both scheduling allocation and energy allocation. Due to the instability of PV energy supply and the uncertainty of completion time due to the workshop scheduling allocation, the aim of this phase is to generate an initial FJSP scheduling solution to provide a time window for subsequent PV energy estimation.

Traditional FJSP scheduling mainly considers the completion time, and in this paper, we introduce the energy weight matrix We ∈ R24, which represents the cost of energy usage for 24 h. In task allocation, time efficiency, energy cost, and carbon emission are combined for comprehensive consideration, and the comprehensive decision function for task allocation is defined as

$$S(j,m,t) = \alpha \cdot f_{time}(j,m) + \beta \cdot f_{energy}(j,m,t) + \gamma \cdot f_{carbon}(j,m,t) \quad (24)$$

where $f_{time}(j,m)$ denotes the time efficiency function of task j on machine m, $f_{energy}(j,m,t)$ denotes the energy cost function, $f_{carbon}(j,m,t)$ denotes the carbon emission function, and α, β, and γ are the weighting coefficients.

After the decision of task allocation is achieved, NSGA-II is used for initial optimization of the objectives, which includes problem encoding and decoding, population

initialization, objective function evaluation, fitness evaluation and selection, and performance of crossover and mutation operations.

A series of non-dominated solutions are generated during the iterative process of NSGA-II, and based on the decision maker's preference, a solution that balances the three objectives is selected as the output of the first stage, with the selection criteria being

$$S_{selected} = \arg\min \left(w_1 \cdot \frac{C_{max}(S) - C_{max}^{min}}{C_{max}^{max} - C_{max}^{min}} + w_2 \cdot \frac{C_{energy}(S) - C_{energy}^{min}}{C_{energy}^{max} - C_{energy}^{min}} + w_3 \cdot \frac{C_{carbon}(S) - C_{carbon}^{min}}{C_{carbon}^{max} - C_{carbon}^{min}} \right), \ S \in \Omega \quad (25)$$

where Ω is the Pareto solution set, and $w_1 = 1/3$, $w_2 = 1/3$, and $w_3 = 1/3$ are the weights of each objective.

3.1.2. PV Availability Estimation

In this section, the approximate energy from PV energy needs to be calculated to provide more accurate energy constraints for the third stage of optimization, introducing buffer parameters

$$buffer = a \cdot C_{max} + b \cdot T_{days} \quad (26)$$

where a and b are adjustable parameters; $a = 0.1$, and $b = 2$. The buffer parameter is used in the third stage to allow the optimized scheduling to extend the completion time within a certain range for better energy utilization.

After obtaining the buffer time, the total available PV energy can be calculated for the entire production cycle:

$$E_{PV,total} = \sum_{t=1}^{C_{max}} Pv(t) \quad (27)$$

Dual optimization of completion time and energy use can be accomplished in the third phase after transforming the unstable PV energy into a controllable amount of PV energy available.

3.1.3. MOPSO Two-Layer Co-Optimization

To address the complexity of joint production-microgrid scheduling, this paper establishes a bi-level optimization framework based on decomposition-coordination, decoupling the model into two interactive mathematical sub-problems. The upper level serves as the master problem, solving the flexible job shop scheduling problem by optimizing machine allocation M and operation timing T to determine the power load profile P_{load}. The lower level acts as the sub-problem for energy management and constraint validation. Upon detecting power balance violations, it calculates Lagrangian multipliers (shadow prices) as feedback. The two levels are coupled via a "prediction-correction" loop (Figure 3): adaptive penalty signals from the lower level compel the upper level to reconfigure load distribution in subsequent iterations, driving the system toward an equilibrium that satisfies constraints from both domains.

(1) Based on Optimal Scheduling of Energy Cost

Extract the energy management scheme X_e for the current particles and calculate the comprehensive energy cost for each time period t and each machine m. The comprehensive energy cost $c_{t,m}$ is as follows:

$$c_{t,m} = w_4 \cdot p_t + w_5 \cdot (1 - \frac{Pv_t}{P_{max}}) + w_6 \cdot (1 - \frac{SOC_t - SOC_{min}}{SOC_{max} - SOC_{min}}) + \eta \cdot \delta_t \quad (28)$$

where P_t is the electricity price in time period t, Pv_t is the PV power in time period t, SOC_t is the state of the energy storage system in time period t, δ_t is the carbon emission intensity in time period t, and w_4, w_5, w_6, and η are the weighting coefficients.

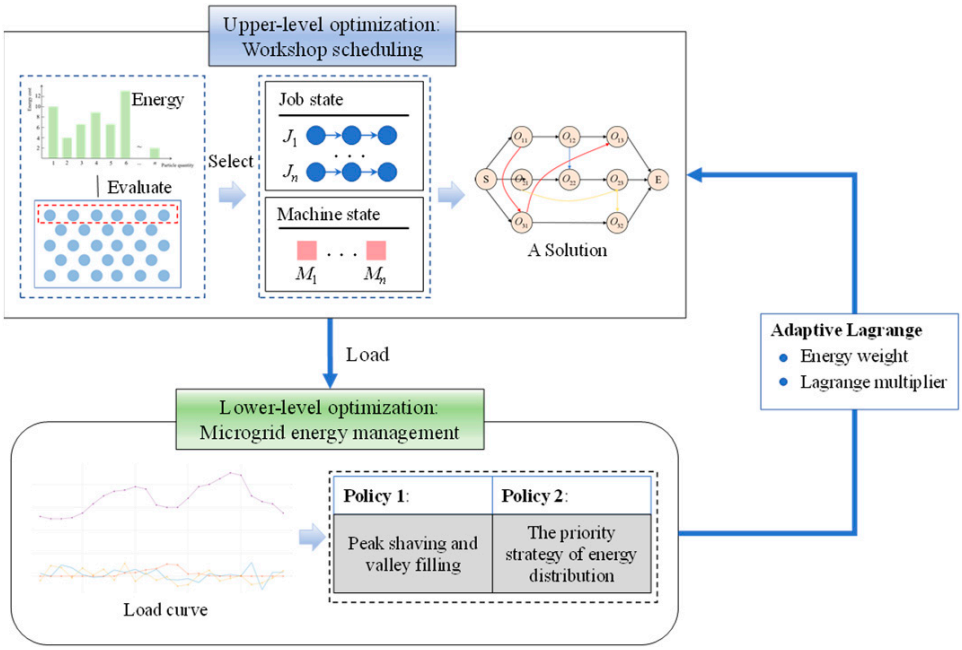


Figure 3. Two-tier collaborative optimization framework.

Simultaneously, evaluate the scheduling and calculate the energy cost for each process j under the current allocation E_j:

$$E_j = \sum_{t=t_j}^{t_j+p_j} c_{t,m_j} \cdot P_{m_j} \tag{29}$$

where t_j is the start time of process j, p_j is the processing time of process j, m_j is the machine assigned to process j, and Pm_j is the power of machine m_j.

The processes are arranged in descending order of energy cost to obtain the candidate optimization process ensemble $\Omega = j_1, j_2, \ldots j_k$. The high energy cost processes are prioritized and adjusted, the high energy cost processes are guided by the energy weights, and the k_s process is selected.

$$k_s = \max(1, \lceil W_e(t) \cdot n \rceil) \tag{30}$$

where $W_e(t)$ is the energy weight, and n is the total number of processes.

For each candidate process $j \in \Omega$, the following adjustment strategy is tried.

(1) Obtain the ensemble of all available machines $M_j = m_1, m_2, \ldots, m_l$ for each available machine, compute the energy cost $E_j(m)$, try to select the machine with the lowest energy cost $m^* = \arg\min_{m \in MjEj}(m)$, and if $E_j(m) < E_j(m_j)$, reassign process j to machine m^*.

(2) Calculate the time window $[S_{ij}, C_{ij}]$ for process j, satisfying process dependencies and machine availability. For each possible machine time t within the window calculate the energy cost $E_j(m)$ and select the start time with the lowest energy cost $t^* = \arg\min_{[ESj,LSj]} E_j(m)$; if $E_j(t) < E_j(t_j)$, adjust the start time of process j to t^*.

After updating the particle locations, a fitness assessment is performed for each particle, applying penalties to processes in high-cost or high-emission time periods and directing scheduling to adjust to low-tariff or high-PV-availability time periods. At the same time, the non-dominated solution is deposited in the warehouse.

(2) Optimizing Energy Management Based on Dispatch

Treating the load profile P_{load} from the upper level as an input boundary, the lower-level microgrid solves the sub-problem targeting minimum operational costs to validate energy-side feasibility. By optimizing battery output P_{Bess} and grid interaction P_{grid}, the system quantifies the power imbalance ΔP (constraint violation), which serves as the quantitative basis for updating Lagrangian multipliers.

$$P_{Load}^{peak} = \left\{ t \middle| P_{Load}(t) > \theta_{peak} \cdot \max(P_{Load}) \right\} \tag{31}$$

$$P_{Load}^{valley} = \left\{ t \middle| P_{Load}(t) < \theta_{valley} \cdot \max(P_{Load}) \right\} \tag{32}$$

where P_{peak} and P_{valley} are the peak and valley determination thresholds, respectively. The peak and valley identification provides the decision basis for the subsequent peak-shaving and valley-filling strategies.

In order to realize the energy system dispatch and grid interaction to achieve smoothing of the load curve, the strategy of charging in the low valley and discharging in the peak period is used in this section.

$$P_{fill}(t) = \begin{cases} \min\left(-P_{ess}^{\min}, \frac{SOC_{\max} - SOC(t)}{\eta_c \times \Delta t}\right), & if\ t \in P_{Load}^{valley} \\ 0, & otherwise \end{cases} \tag{33}$$

$$P_{out}(t) = \begin{cases} \min(P_{load}(t) - P_{pv}(t), P_{ess}^{\max}, \frac{(SOC(t) - SOC_{\min}) \times \eta_d}{\Delta t}, & if\ t \in P_{Load}^{peak} \\ 0, & otherwise \end{cases} \tag{34}$$

At the same time, based on the characteristics of the PV cell and load demand, establish a priority strategy for energy distribution: prioritize the use of the PV cell to meet load demand and maximize utilization of renewable energy.

$$P_{\text{used}}(t) = \min\left(P_{\text{pv}}(t), P_{\text{load}}(t)\right) \tag{35}$$

If there is a surplus of PV energy, the excess PV power is stored in the energy storage system.

$$P_{surplus}(t) = \max(0, P_{pv}(t) - P_{Load}(t)) \tag{36}$$

$$P_{\text{charge}}(t) = \min\left(P_{\text{surplus}}(t),\ -P_{\text{ess}}^{\min},\ \frac{SOC_{\max} - SOC(t)}{\eta_+ \cdot \Delta t}\right) \tag{37}$$

When load demand exceeds PV supply, energy storage systems are prioritized to make up the difference.

$$P_{\text{surplus}}(t) = \max(0, P_{\text{Load}}(t) - P_{\text{pv}}(t)) \tag{38}$$

$$P_{\text{discharge}}(t) = \min\left(P_{\text{load_surplus}}(t),\ P_{\text{ess}}^{\max},\ \frac{(SOC(t) - SOC_{\min}) \cdot \eta_d}{\Delta t}\right) \tag{39}$$

Power is purchased from the main grid when the energy storage system is unable to meet demand.

$$P_{\text{grid}}(t) = P_{\text{load}}(t) - P_{\text{used}}(t) - P_{\text{discharge}}(t) \tag{40}$$

$$\Delta P(t) = \left| \sum_m P_L(t,m) - P_{pv}(t) - \sum_m P_{bess}(t,m) - \sum_m P_{grid}(t,m) \right| \tag{41}$$

$\Delta P(t)$ quantifies the deviation from microgrid physical constraints, serving as the core coupling variable for the master-sub-problem iteration. To drive the upper-level schedule toward the energy feasible region, these physical "hard" violations must be translated into

economic "soft" penalties within the objective function. Leveraging Lagrangian relaxation, $\Delta P(t)$ is mapped to dynamic Lagrangian multipliers, establishing a feedback mechanism between the scheduling and energy layers. The specific adaptive update strategy is detailed in Section 3.2.

3.2. Adaptive Lagrangian Feedback Mechanism

Aiming at coupling challenges in the smart manufacturing and microgrid integration optimization problem, this paper proposes a feedback optimization framework based on the adaptive Lagrangian multiplier method. The method coordinates the mutual influence between production scheduling and energy management by dynamically adjusting energy weights to achieve efficient convergence of multi-objective optimization.

3.2.1. Lagrangian Function Construction

The augmented Lagrangian function is constructed for the power balance constraints

$$L_A(x, \lambda, \rho) = F(x) + \lambda^T v(x) + \frac{\rho}{2} \| v(x) \|^2 \tag{42}$$

where λ is the Lagrange multiplier vector, and ρ is the penalty factor. $v(x)$ denotes the degree of power balance violation.

3.2.2. Adaptive Weight Updating

To mitigate numerical oscillations often encountered with standard sub-gradient methods, we design an adaptive damping mechanism comprising two key steps to dynamically regulate the step size η^k and penalty factor ρ^k.

(1) Oscillation Detection and Parameter Adaptation.

The mechanism first evaluates the constraint violation norm $\Delta v^k = \| v\left(x^k\right) \|$. If $\Delta v^k > \Delta v^{k-1}$ (violation increases), indicating trajectory oscillation, a damping phase is triggered: the step size is decayed ($\eta^{k+1} = \gamma_{dec} \cdot \eta^k$), and the penalty factor ρ is boosted to force the search back into the feasible region. Conversely, if $\Delta v^k \leq \Delta v^{k-1}$, the convergence is deemed stable, and the step size is increased to accelerate optimization.

(2) Augmented Weight Update.

Incorporating the adapted parameters and the augmented Lagrangian first-order necessary conditions, the energy weight update is formulated as

$$w_t^{k+1} = \mathcal{P}_\Omega \left(w_t^k + \eta^k \cdot v_t\left(x^k\right) + \rho^k \cdot \left(v_t\left(x^k\right) \right)^2 + \alpha \cdot d_t \right) \tag{43}$$

Here, the augmented quadratic feedback term $\rho^k \cdot (v_t(x^k))^2$ provides non-linear suppression of large deviations. This is complemented by the momentum term $\alpha \cdot d_t$ (Equation (42)), which utilizes historical information to smooth the update trajectory and enhance convergence robustness.

3.2.3. Adaptive Parameter Adjustment

In order to improve optimization efficiency and stability, an adaptive parameter adjustment strategy is adopted, with the following steps:

(1) Adaptive step size adjustment

$$\eta^{k+1} = \begin{cases} \min(\eta_{\max}, \eta^k \cdot 1.1), \ if \ v(x^k) < v(x^{k-1}) \\ \max(\eta_{\min}, \eta^k \cdot 0.9), \ otherwise \end{cases} \tag{44}$$

(2) Adaptive penalty factor adjustment

$$\rho^{k+1} = \begin{cases} \max(\rho_{\min}, \rho^k \cdot 0.9), & if\ v(x^k) < 0.5 \cdot v(x^{k-1}) \\ \min(\rho_{\max}, \rho^k \cdot 1.2), & if\ v(x^k) > v(x^{k-1}) \\ \rho^k, & otherwise \end{cases} \tag{45}$$

(3) Local most-jumping-out mechanism

When the violation varies very little over many consecutive iterations, the step size is increased to jump out of the local optimum:

$$\eta^{k+1} = \min(\eta_{\max}, \eta^k \cdot 1.5) \tag{46}$$

This feedback is used as a condition for aborting the iteration on one of the following convergence criteria:

(1) The amount of weight change is less than the threshold:

$$\frac{\left\| \lambda^k - \lambda^{k-1} \right\|}{\lambda^{k-1}} < \xi_{total} \tag{47}$$

(2) The power balance constraint violation is less than the allowable value:

$$\left\| v(x^k) \right\| < \xi_v \tag{48}$$

(3) The maximum number of iterations is reached:

$$k > k_{\max} \tag{49}$$

The updated energy weights are fed back to the upper layer to increase the adaptation penalties for high violation or high electricity price periods in the next round of MOPSO iterations, guiding the scheduling to adjust to low-cost and low-emission periods.

3.3. Problem Coding and Decoding

The three-stage hierarchical optimization framework proposed in this paper requires joint coding of the FJSP and the microgrid energy management problem. Since the scheduling problem is a discrete problem, and microgrid management is a continuous problem, a hybrid coding scheme is designed to be able to represent both the production scheduling decision and the energy management strategy. An example of a scheduling job with three artifacts and two machines is shown in Figure 4.

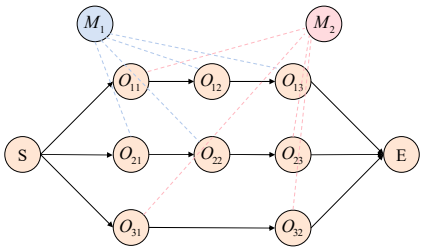


Figure 4. Heterogeneous map of scheduling cases.

The heterogeneous diagram in the figure shows the scheduling state of the case, with the dashed lines indicating the available machines, while the solid lines indicate the order of processing. A coding scheme constructed for the scheduling case is shown in Figure 5.

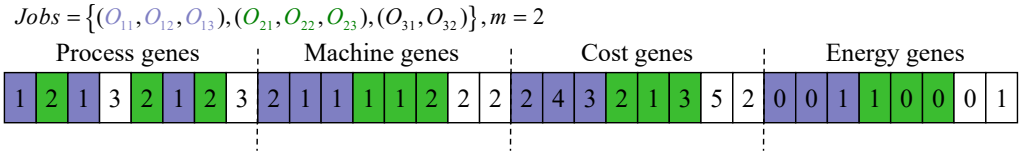


Figure 5. Four-layer coding scheme.

Figure 5 illustrates an example coding scheme consisting of four different genes. The process gene indicates the number of times the workpieces are processed and the order in which they are processed; the machine gene controls the allocation of the machine; the energy consumption gene represents the amount of energy required for the processing of the workpieces; and the energy gene controls whether or not photovoltaic energy is used in the processing of the workpieces. A 1 indicates that photovoltaic energy is used, while a 0 indicates that the energy is supplied by the grid.

Figure 6 shows the coding scheme of the example case composition, which is plotted in the form of a Gantt chart for the sake of clear description, with the left y-axis, x-axis, and right y-axis denoting the machine selection, the processing time, and the energy consumption, respectively. When the first process gene assigns the operation of workpiece 1, then the machine gene will immediately follow by assigning the corresponding workpiece to machine 2. When the operation is executed, the energy consumption of the assigned process is calculated, and it is determined whether the process should be powered by photovoltaic or not. With this coding scheme, this complex integrated optimization problem can be effectively transformed into a solvable mathematical model.

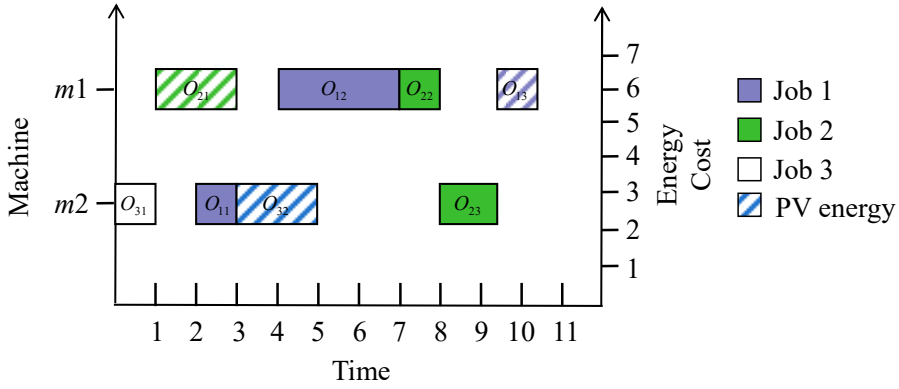


Figure 6. Gantt chart of coding scheme composition.

3.4. Improvement of the MOPSO Algorithm

3.4.1. Chaotic Mapping

Chaotic systems are highly sensitive to initial conditions, both non-periodic and ergodic, and are capable of generating pseudo-random dynamic sequences in a finite space. Compared with traditional uniform random mapping, chaotic mapping can provide a more uniform search trajectory and avoid the search process falling into the local optimal region. In particle swarm optimization, random coefficients have an important impact on search behavior. Uniform distribution of traditional random coefficients may lead to too-homogeneous search behavior, while chaotic mapping can introduce nonlinear dynamics and enhance global search capability. In this paper, a logistic map is used as the implementation of chaotic mapping, and its mathematical expression is

$$x_{n+1} = \mu \cdot x_n \cdot (1 - x_n) \tag{50}$$

where μ is a control parameter. When $\mu = 4$, the Logistic Map exhibits completely chaotic behavior and generates a sequence with good traversal in the range [0, 1]. This chaotic sequence is used to generate the stochastic coefficients in the particle velocity update formulation, thus enhancing the exploration capability of the particle swarm.

By integrating chaotic mapping into the velocity update process of MOPSO, the improved velocity update equation is

$$v_{i,j}^{t+1} = \xi_{1,j}^{t} \cdot v_{i,j}^{t} + \xi_{2,j}^{t} \cdot \left(x_{\text{winner},j}^{t} - x_{i,j}^{t} \right) \tag{51}$$

where $\xi_{1,j}^{t}$ is the chaos coefficient in the jth dimension of the tth generation,$x_{winner,j}^{t}$ is the jth dimensional position of the leader particle selected through a competitive mechanism, and the production of chaos coefficients follows a logistic mapping progression

$$\xi_{k,j}^{t} = 4\xi_{k,j}^{t-1}\left(1 - \xi_{k,j}^{t-1}\right), \quad k \in \{1, 2\} \tag{52}$$

where the initial chaos value $\xi_{k,j}^{0}$ is chosen randomly in the interval (0, 1) and $\xi_{k,j}^{0} \neq 0.5$ to avoid immobile points.

3.4.2. Adaptive Mutation

In multi-objective optimization, maintenance of population diversity is crucial for obtaining high-quality Pareto frontiers. Conventional MOPSO's mutation operation usually uses fixed mutation probabilities and distribution indices, which are difficult to adapt to the needs of different optimization stages. For example, a large magnitude of variation is needed at the early stage to facilitate exploration, while a smaller magnitude of variation is needed at the later stage to fine-tune the solution. Therefore, this paper proposes an adaptive mutation strategy that adapts to the needs of the optimization process by dynamically adjusting the mutation probability and distribution index.

The mutation probability decreases linearly based on an iterative progress, with a high probability in the early stage to promote the global search, and a low probability in the later stage to focus on the local exploitation. Its mathematical expression is as follows:

$$p_m^t = p_{m,\max} - (p_{m,\max} - p_{m,\min}) \cdot \frac{t}{T} \tag{53}$$

where p_m^t is the mutation probability at generation t, $p_{m,\max}$ and $p_{m,\min}$ are the upper and lower bounds of the mutation probability, respectively, and T is the maximum number of iterations.

The distribution index is dynamically adjusted according to the crowding distance of the population, and the magnitude of variation is increased when the population diversity is low to maintain the distributivity of the solution.

An improved crowding distance is used as a quantitative index of population diversity, and for the ith individual, the crowding distance is defined as

$$CD_i = \sum_{m=1}^{M} \frac{f_m^{i+1} - f_m^{i-1}}{f_m^{\max} - f_m^{\min}} \tag{54}$$

where M is the number of objective functions, and $f_m^{\max}$ and $f_m^{\min}$ are the maximum and minimum values of the mth objective, respectively.

Indicators of overall population diversity are defined as

$$D^t = \frac{\overline{CD^t}}{CD_{\max^t}} \tag{55}$$

where $\overline{CD^t}$ and $CD_{\max^t}$ are the average and maximum crowding distances of the population, respectively.

Based on the population diversity, the adaptive formula for the distribution index is

$$\eta_m^t = \eta_{m,\min} + (\eta_{m,\max} - \eta_{m,\min}) \cdot (1 - D^t) \tag{56}$$

where $\eta_{m,max}$ and $\eta_{m,max}$ are the upper and lower bounds of the distribution index, respectively.

For each particle's dimension, the probability P_m determines whether it is mutated or not, with the following mathematical expression:

$$\begin{cases} x'_{i,j} = x_{i,j} + (x_{j,\max} - x_{j,\min}) \cdot \left[\left(2u_{i,j} + (1 - 2u_{i,j}) \left(1 - \frac{x_{i,j} - x_{j,\min}}{x_{j,\max} - x_{j,\min}} \right)^{\eta_m^t + 1} \right)^{\frac{1}{\eta_m^t + 1}} - 1 \right], & if\ u > 0.5 \\ x'_{i,j} = x_{i,j} + (x_{j,\max} - x_{j,\min}) \cdot \left[1 - \left(2(1 - u_{i,j}) + 2(u_{i,j} - 0.5) \left(1 - \frac{x_{j,\max} - x_{i,j}}{x_{j,\max} - x_{j,\min}} \right)^{\eta_m^t + 1} \right)^{\frac{1}{\eta_m^t + 1}} \right], & otherwise \end{cases} \tag{57}$$

3.4.3. CMOPSO Algorithm Solution Flow

The algorithm flow of CMOPSO is shown in Figure 7, where blue represents the original MOPSO flow, orange represents the improved part, and green is the judgment statement.

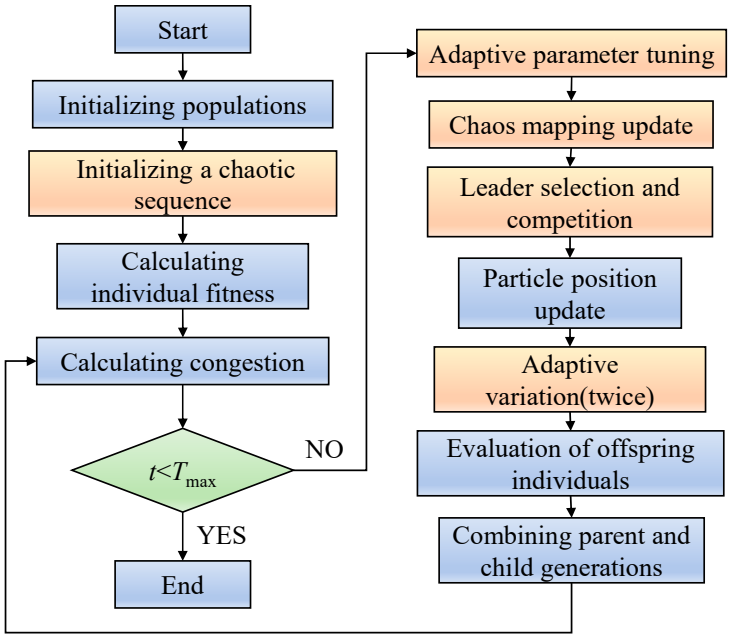


Figure 7. Improved multi-objective particle swarm algorithm flow.

4. Case Validation

In this section, sufficient experiments are designed to validate the performance of the proposed algorithms. The simulations were conducted in MATLAB 2023a on a workstation equipped with an AMD Ryzen 9 7940H CPU (3.4 GHz), 16 GB RAM, and an NVIDIA RTX 4060 GPU. Regarding the algorithm configuration, the key parameters of CMOPSO were determined by referring to standard settings in the literature [32] and conducting preliminary sensitivity tests. Specifically, the population size is set to 100, the maximum number of iterations is 100, the inertia weight w is 0.5, and the acceleration coefficients are set to c_1 = 1.5 and c_2 = 1.5. The remaining parameters were configured in accordance with the recommendations provided in [32]. Furthermore, the physical specifications of the microgrid components and the time-of-use tariff data used in the case study are derived

from typical industrial standards and local commercial pricing policies, respectively, as detailed in Section 2.1.2.

4.1. Case Background

To validate the three-stage multi-objective optimization model and its solution proposed in this paper, the test set provided by Brandimate [33] was used as a benchmark. Table 3 shows an example of the benchmark example MK01, which contains 10 jobs and six machines.

Table 3. Processing power per machine.

Machine	Processing	Idle	Machine	Processing	Idle
M1	2	0.6	M4	2.4	0.4
M2	1.6	0.6	M5	2.4	0.4
M3	1.8	0.5	M6	4.1	0.6

In order to place the cases in the context of considering the dispatch of a PV microgrid, for the different cases, an energy storage system with a capacity of 150 kWh is designed, which has a charging and discharging power of 10 kW and 12 kW, respectively. It is assumed that there exists a distributed solar panel for the shop floor to carry out the generation of the energy, which generates a peak of 6000 kWh. these values are based on a real PV system. For different cases, the real values are scaled to fit the actual supply in performing the workshop generation activities.

4.2. Experimental Results

In order to analyze the effectiveness of the algorithm in the case, specific to the MK01 case, the algorithm generates a non-dominated Pareto frontier, as shown in Figure 8, with the convergence curve shown in Figure 9.

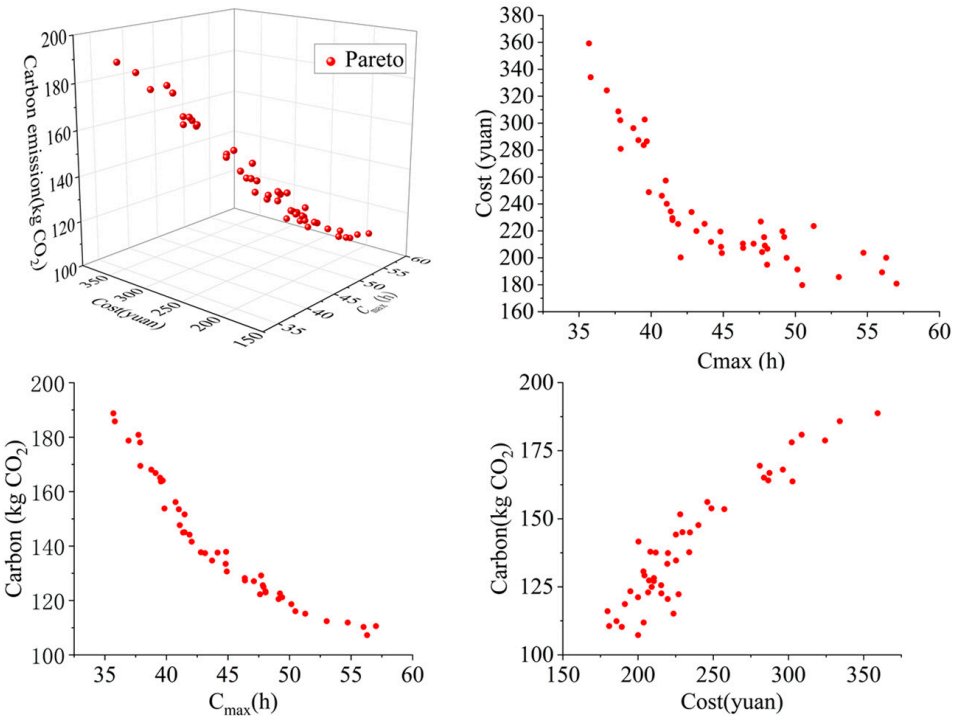


Figure 8. Pareto frontier based on the triple objective.

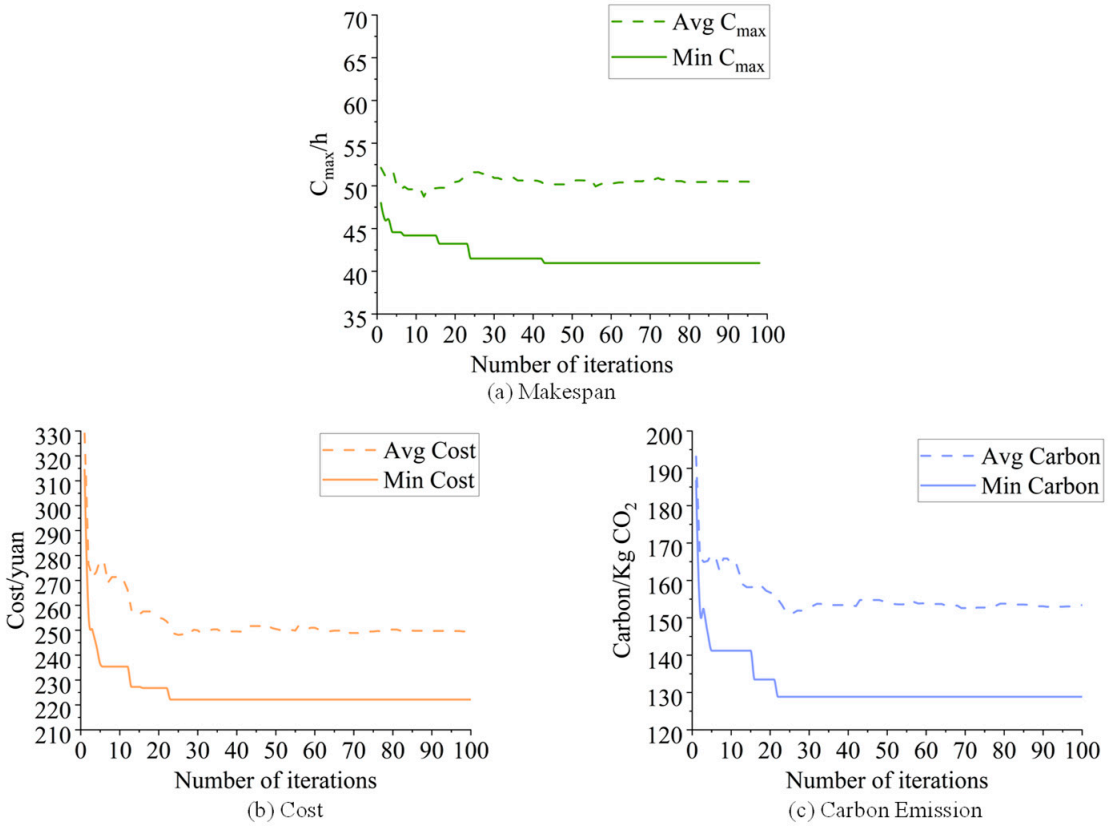


Figure 9. Iterative convergence curves for different objectives.

From Figure 9, it can be learned that the carbon emission and cost converged in 25 generations, and the completion time converged in 50 generations. The initial solution of the completion time is lower, which is due to the initial scheduling in the first stage, and the solution with larger completion time will be preferentially excluded in the third stage of optimization.

The three objectives are evaluated using linear weighting, where each objective function has a weight of 1/3, from which the optimal scheduling under the equilibrium decision can be obtained. The scheduling scheme is shown in Figure 10.

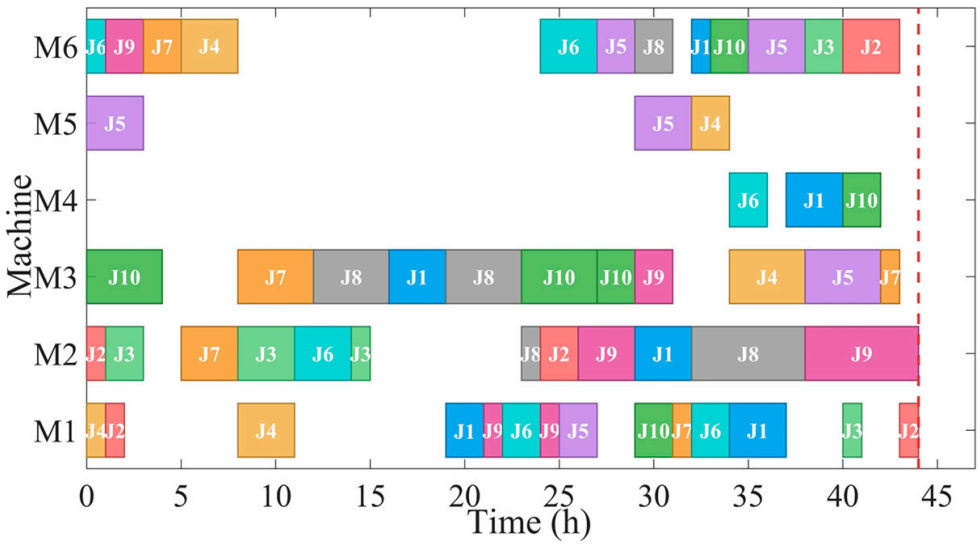


Figure 10. *Cont.*

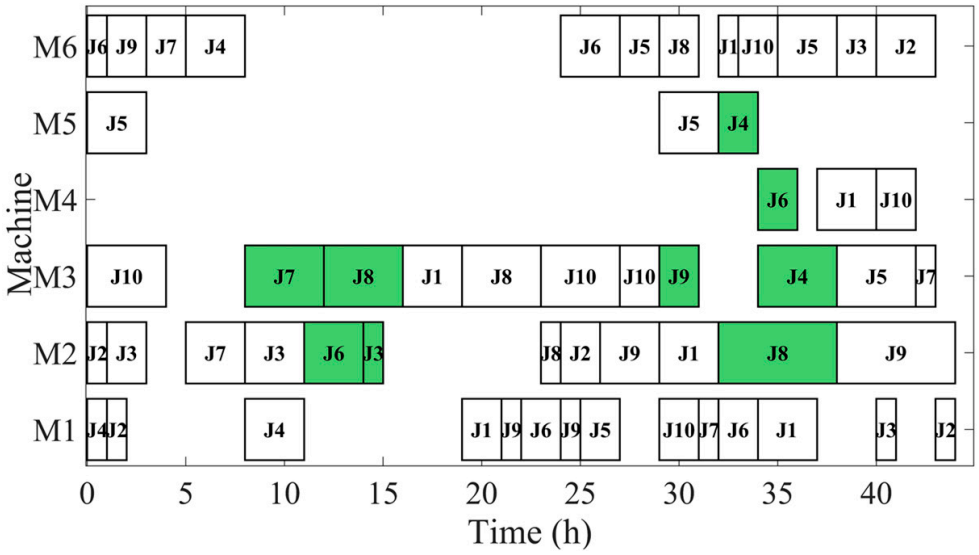


Figure 10. Scheduling results of the balanced program.

From the analysis of the scheduling scheme, it can be seen that PV power generation and the tariff period show an isotropic effect. Since PV production capacity is mainly concentrated in the daytime hours with sufficient light, which coincides with the flat and peak periods of the electricity price, PV power is basically realized as soon as it is generated, and there is seldom any transfer of the power surplus to the subsequent periods. At the same time, the production scheduling also reflects a clear cost orientation, which effectively reduces overall costs by scheduling the main processing hours in the low tariff zone.

In order to enable the decision maker to choose the appropriate solution according to personal preference, for the three objectives, we consider three different extreme cases, which are cases where the decision preference is for minimum completion time, minimum cost, and minimum carbon emission. Figures 11–13 show the microgrid energy allocation diagrams for the three extreme cases, as well as the grid output power and tariff interaction diagrams.

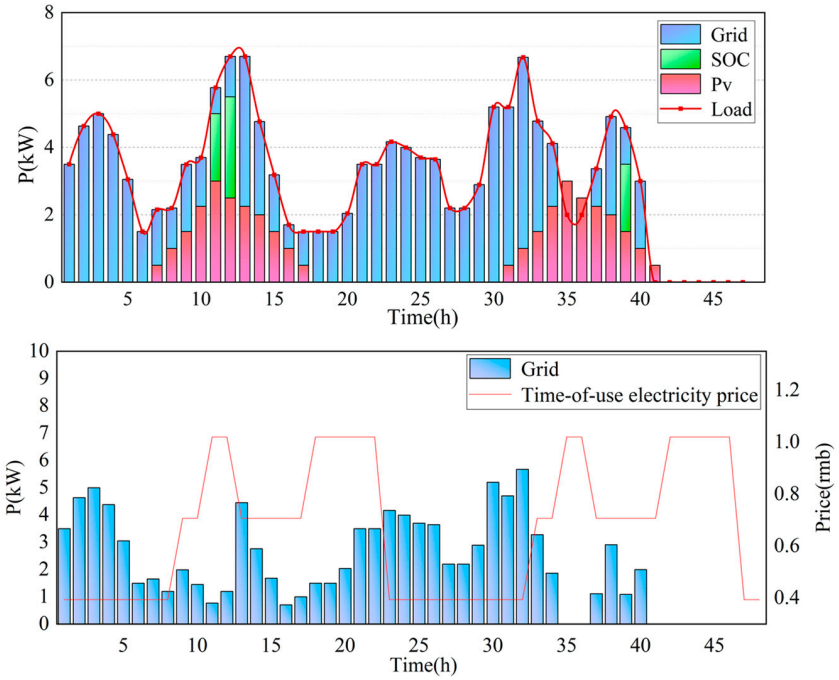


Figure 11. Preferred time of completion.

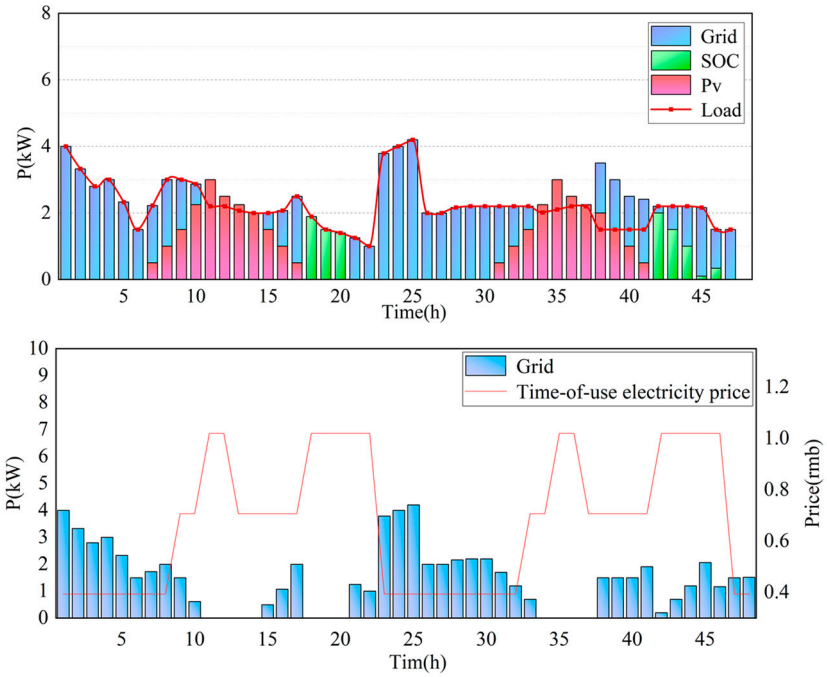


Figure 12. Preferred costs.

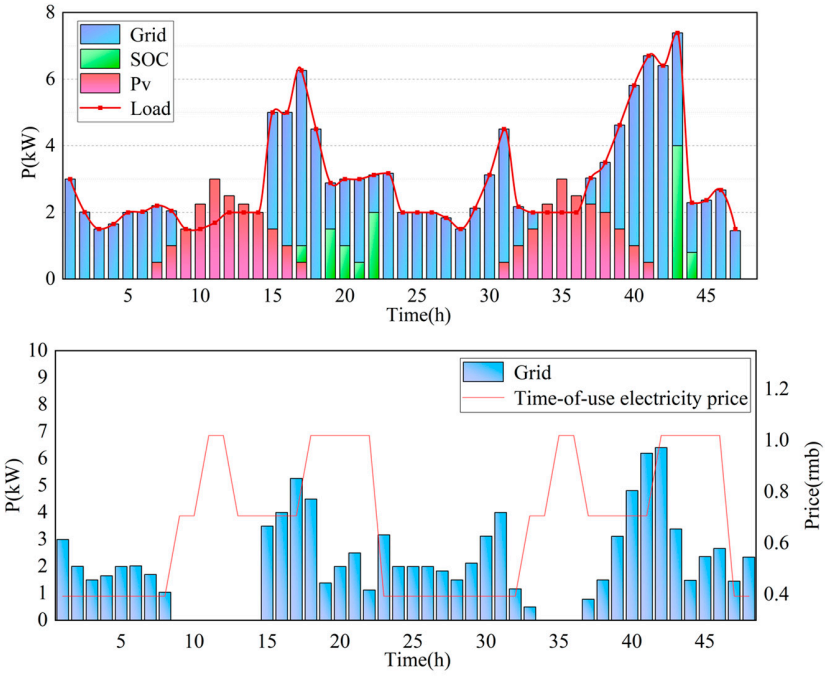


Figure 13. Preferred carbon emissions.

Under the decision preference of completion time priority, the scheduling system achieves efficient scheduling of centralized processing by optimizing the time between processes. However, the use of photovoltaic energy is still prioritized during high electricity price hours, and the decision is made to reduce energy costs by shifting energy-intensive tasks to flat and low valley electricity price hours.

Under the cost-first decision-making preference, the time-sharing tariff strategy guides the plant to utilize more PV renewable energy during peak hours, reducing reliance on grid power and lowering carbon emissions and costs. At the same time, it reduces peak power consumption and increases valley power consumption by optimizing the power consumption plan and shifting high-load production tasks to low or flat hours.

Under the decision of preferring carbon emissions, the dispatch scheme guides the high-load tasks to be processed in the low or flat tariff hours through the time-sharing tariff strategy and prioritizes the use of energy storage devices to supply power in peak tariff hours in order to reduce the carbon emissions of the scheme, but some high-load tasks are still scheduled in peak hours due to the constraints of the time of completion.

From analysis of the MK01 case, it can be concluded that the method can effectively optimize scheduling while taking into account energy allocation in the microgrid and using the time-sharing tariff strategy to achieve double optimization of both time and energy levels.

4.3. Comparison of Algorithms

In order to verify the effectiveness of the algorithm, the CMOPSO algorithm is compared with the MOPSO algorithm, the NSGA-II [34] algorithm, and the SPEA-II [35] algorithm, and the optimal solution of multiple runs is selected by the Analytic Hierarchy Process (AHP) [36] under the condition of the same parameter. The bold font represents the optimal solution of four algorithms. The objective value is optimal, as shown in Table 4.

Table 4. Comparison of the objectives of different algorithms, using Brandimarte calculus.

Case	Indicator	CMOPSO	MOPSO	NSGA-II	SPEA-II
MK01	$f1$	**40**	45	41	47
	$f2$	182.5	197.7	**161.8**	185.7
	$f3$	**240.2**	271.4	282	259.1
MK02	$f1$	**42**	50	50	46
	$f2$	**189.6**	197.7	213.6	243.27
	$f3$	**259.9**	274.8	304.5	289.74
MK03	$f1$	**157**	182	179	173
	$f2$	**823.5**	874.3	862.2	849.3
	$f3$	**1083.8**	1199.4	1095.4	1120.6
MK04	$f1$	**105**	120	129	112
	$f2$	**387.1**	405	406.5	419.5
	$f3$	521.6	546.2	**510.5**	547.8
MK05	$f1$	**208**	226	214	214
	$f2$	**442.6**	462.3	468.1	470.8
	$f3$	**601.6**	620.3	601.8	650.4
MK06	$f1$	**109**	116	110	122
	$f2$	**732.6**	777	789.8	743.2
	$f3$	**959**	1055	1022	981
MK07	$f1$	176	**165**	185	197
	$f2$	**671**	691.9	684.1	700.6
	$f3$	**887.5**	906.3	948.9	924.9
MK08	$f1$	591	613	594	**588**
	$f2$	**2491.3**	2515.5	2544.8	2528.6
	$f3$	**3314.2**	3353.8	3373.4	3372.1
MK09	$f1$	**442**	452	460	**442**
	$f2$	**2014.4**	2027.5	2031.5	2063.8
	$f3$	**2553.9**	2768.8	2631.3	2760.8
MK10	$f1$	**326**	351	344	339
	$f2$	**1187.7**	1220.1	1200.7	1236.7
	$f3$	**1610.4**	1638.6	1615.8	1670.1

Table 4 presents a quantitative comparison of the optimal objective values obtained by the four algorithms across ten benchmark instances (MK01–MK10), ranging from small-scale to large-scale problems. The bold values highlight the best results among the compared methods. Taking the MK01 instance as an example, CMOPSO achieves the minimum values in terms of makespan (40), cost (182.5), and carbon emissions (240.2), which are significantly lower than those of the baseline MOPSO (45, 197.7, 271.4) and NSGA-II. Furthermore, in large-scale instances such as MK06 and MK10, CMOPSO consistently maintains its dominance. This indicates that the proposed algorithm, enhanced by chaotic mapping and adaptive strategies, possesses superior global search capabilities and stability, effectively avoiding local optima compared to traditional algorithms.

In order to further compare the performance of the algorithms, the four algorithms are each run randomly on the small-sized arithmetic case MK01, the medium-sized arithmetic case MK04, and the large-sized arithmetic case MK06, and the derived Pareto fronts are plotted, as shown in Figure 14. There are more non-dominated solutions solved by CMOPSO than by the other three algorithms, and the non-dominated solution space corresponding to them is more centralized, which suggests that this paper's CMOPSO has better convergence.

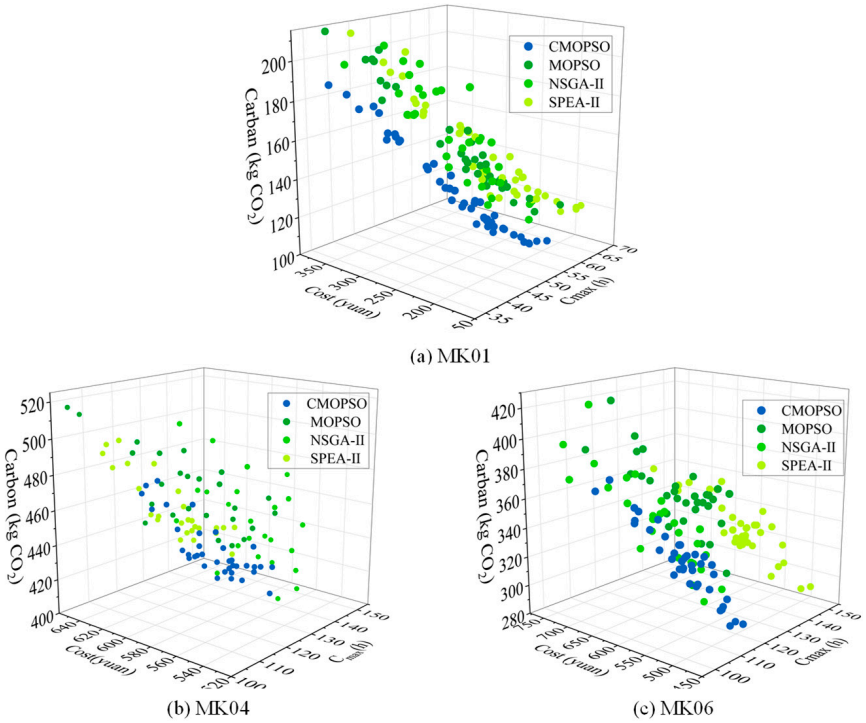


Figure 14. Comparison of different algorithmic Pareto fronts.

4.3.1. Performance Evaluation Metrics

When evaluating the performance of an algorithm, it is crucial to consider multiple aspects. In this paper, the performance of the algorithm is comprehensively evaluated by the following metrics [37].

(1) IGD (inverted generational distance) evaluates the convergence performance and distribution performance of the algorithm by calculating the minimum sum of the distances between each individual to the set of individuals acquired by the algorithm on the real Pareto fronts. The smaller the value, the better the comprehensive performance of the algorithm, including convergence and distribution performance. The formula is as follows:

$$IGD(P,Q) = \frac{\sum_{v \in P} d(v,Q)}{|P|} \quad (58)$$

where P is the set of points uniformly distributed on the true Pareto surface, $|P|$ is the number of individuals in the set of points distributed on the true Pareto surface, Q is the set of the most Pareto-optimal solutions obtained by the algorithm, and $d(v,Q)$ is the minimum Euclidean distance from individual v in P to population Q.

(2) HV (hypervolume) calculates the hypervolume dominated by the non-dominated solution set in the target space with respect to a certain reference point. HV reflects both the convergence and the distribution of the solution set. The larger the value of HV, the higher the quality of the solution set. The formula is as follows:

$$HV(X,P) = \bigcup_{x \in X} v(x,P) \tag{59}$$

where $v(x,P)$ denotes the hypervolume of the space formed between the solution x and the reference point P in the non-dominated solution set X.

(3) Spread calculates the distribution degree index of the non-dominated solution set generated by the multi-objective optimization algorithm with respect to the real Pareto front, which is a comprehensive measure of the uniformity and coverage of the solution set. A smaller the value indicates that the distribution of the solution set is more uniform and the coverage is more extensive. The formula is as follows:

$$\Delta = \frac{d_1 + \sum_{i=1}^{|A|-1} |d_i - \overline{d}|}{d_1 + (|A| - m)\overline{d}} \tag{60}$$

where $|A|$ is the number of solution sets, m is the number of objective functions, and di denotes the average distance from each solution to the nearest neighbor solution.

A comprehensive assessment of the convergence, coverage, and uniformity of distribution of the algorithm through these metrics provides a more comprehensive understanding of the algorithm performance.

4.3.2. Analysis of Test Results

Thirty runs of the four algorithms were performed with the same parameter settings, and the mean values of the solution set metrics were calculated. The results are shown in Tables 5–7.

Table 5. IGD performance indicators.

Test Function	IGD			
	CMOPSO	**MOPSO**	**NSGA-II**	**SPEA-II**
MK01	**0.439**	0.487	0.535	0.549
MK02	**0.387**	0.440	0.492	0.427
MK03	**0.354**	0.389	0.399	0.460
MK04	**0.409**	0.472	0.458	0.504
MK05	0.425	0.422	**0.367**	0.431
MK06	**0.351**	0.428	0.437	0.424
MK07	**0.317**	0.368	0.335	0.522
MK08	**0.357**	0.370	0.529	0.580
MK09	**0.428**	0.499	0.514	0.492
MK10	**0.256**	0.320	0.366	0.410

Table 6. HV performance indicators.

Test Function	HV			
	CMOPSO	**MOPSO**	**NSGA-II**	**SPEA-II**
MK01	**0.757**	0.556	0.593	0.599
MK02	0.692	**0.731**	0.606	0.516
MK03	**0.704**	0.535	0.694	0.538
MK04	**0.793**	0.618	0.664	0.592
MK05	0.725	**0.734**	0.691	0.560
MK06	**0.811**	0.599	0.574	0.474
MK07	**0.761**	0.609	0.626	0.431
MK08	**0.785**	0.630	0.629	0.679
MK09	0.696	**0.772**	0.651	0.685
MK10	**0.759**	0.598	0.673	0.511

Table 7. Spread performance indicators.

Test Function	Spread			
	CMOPSO	**MOPSO**	**NSGA-II**	**SPEA-II**
MK01	**0.319**	0.440	0.546	0.511
MK02	**0.328**	0.472	0.445	0.508
MK03	**0.345**	0.439	0.375	0.558
MK04	**0.396**	0.490	0.548	0.527
MK05	0.495	0.530	**0.453**	0.567
MK06	**0.323**	0.424	0.541	0.455
MK07	**0.293**	0.485	0.579	0.451
MK08	**0.271**	0.559	0.615	0.389
MK09	**0.257**	0.529	0.515	0.457
MK10	**0.224**	0.423	0.665	0.575

CMOPSO shows excellent performance in terms of all three performance aspects: convergence, coverage, and uniformity of distribution. It is known from the IGD metrics that CMOPSO obtains nine optimal solutions and shows excellent performance in terms of convergence of the solution set, which is only slightly inferior to MOPSO and NSGA-II for the MK05 case. Secondly, its performance in terms of coverage is known from the HV performance metrics of the table, where CMOPSO slightly underperforms MOPSO for the MK09 case. Finally, its performance in terms of uniformity of distribution is proved from the spread performance of the table, where CMOPSO underperforms MK05 only for MK04. In summary, from the performance metrics of all three, CMOPSO shows excellent performance, outperforming the other three algorithms. Taking instances of different scales (MK01, MK04, and MK06) as representative study objects, the comparative boxplots for performance indices IGD, HV, and spread are plotted in Figure 15. To interpret the results, lower values indicate better performance for IGD and spread, while higher values are preferred for HV. As observed in the boxplots, the proposed algorithm achieves median values closer to the ideal optima compared to the baselines. Furthermore, the distribution is more centralized (indicated by the shorter box heights), demonstrating lower variance. These results confirm that the proposed algorithm significantly outperforms the other algorithms in terms of convergence, coverage, and uniformity.

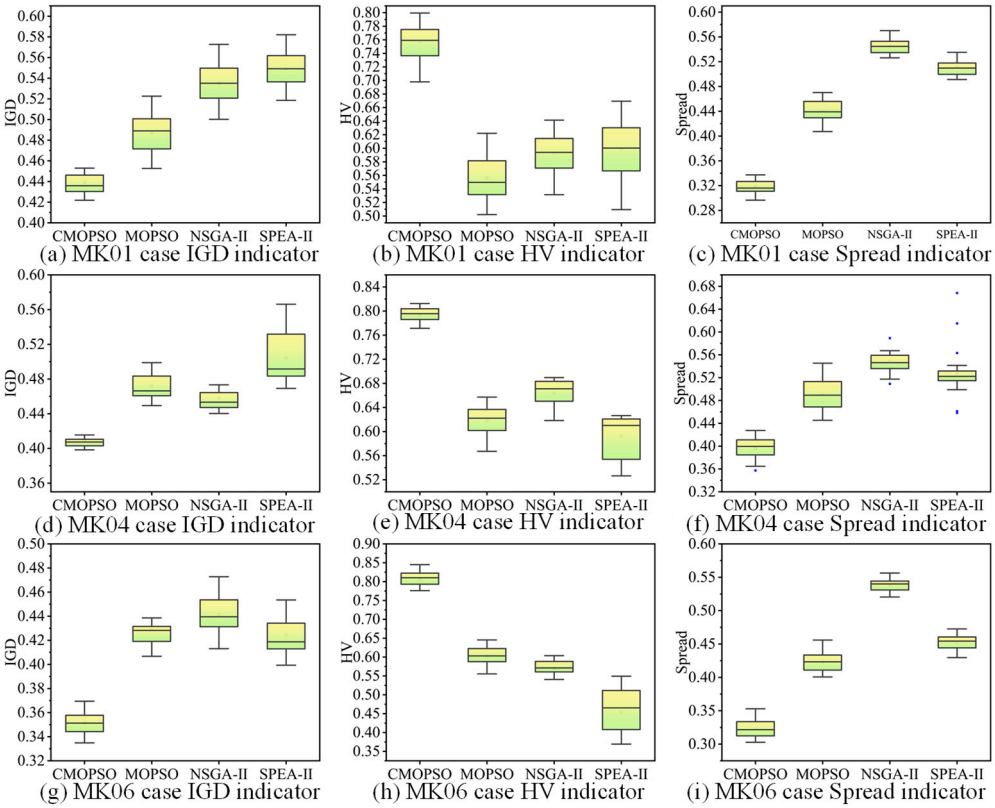


Figure 15. Comparison of boxplots of performance metrics of different algorithms.

4.4. Melting Experiment

To rigorously quantify the individual contributions of the photovoltaic system and the time-of-use pricing strategy in reducing production costs and carbon emissions, and to verify the synergistic effect of their combination, this section designs an ablation study. We construct four progressive scenarios by controlling two variables—-"PV Configuration" and "Pricing Strategy"—-to isolate the impact of each factor.

The four comparative scenarios are defined as follows.

Scenario 1 (with PV + ToU): The complete collaborative model proposed in this paper, incorporating both PV generation and ToU pricing signals. This scenario aims to verify the maximized benefits with "Source-Price" coupling.

Scenario 2 (with PV + flat price): The PV system is installed, but the electricity price remains fixed (mean value). This scenario tests the energy substitution benefit of PV itself, while examining system performance when energy storage operates in a passive fluctuation-smoothing mode due to the lack of price incentives.

Scenario 3 (no PV + ToU): Based on Scenario 4, the ToU pricing strategy is introduced, but still without PV. This scenario aims to test the economic benefits of "peak shaving and valley filling" and load shifting using price signals when relying solely on grid power.

Scenario 4 (baseline: no PV + flat price): This simulates a traditional job shop environment. The microgrid has no PV generation and relies entirely on the external grid. Furthermore, the electricity price is fixed. In this scenario, the system lacks low-carbon energy sources, and the energy storage system has no arbitrage room.

In order to ensure the fairness of the comparative experiment and avoid errors caused by deviations in the setting of the benchmark price, the "fixed electricity price" used in scenarios 2 and 4 is calculated based on the weighted average of the time-of-use electricity price over a 24 h period. The formal calculation formula is as follows:

$$\overline{P} = \frac{\sum_{i=1}^{n} P_i \cdot T_i}{\sum_{i=1}^{n} T_i} \tag{61}$$

where $\overline{P}$ is the average electricity price (yuan/kWh); P_i is the price for the i-th time period (e.g., valley, shoulder, peak); T_i is the duration of the i-th time period (hours); n is the number of distinct time periods (here, $n = 3$), and $\sum_{i=1}^{n} T_i = 24$. The fixed electricity price is calculated as $\overline{P} = 0.668$ yuan/kWh. This setting ensures that the ablation study evaluates the optimization performance.

The comparison results of total electricity cost and carbon emissions in the four scenarios are presented in Table 8.

Table 8. Comparison of ablation study results in different energy scenarios.

Scenario	PV Configuration	Price Strategy	Makespan (h)	Total Cost (Yuan)	Carbon Emissions (kg)	Cost Reduction	Emissions Reduction
1	Installed	ToU Price	40	182.5	240.5	-	-
2	Installed	Flat Price	40	231.2	248.2	21.1%	3.1%
3	None	ToU Price	40	306.6	346.1	40.5%	30.5%
4	None	Flat Price	40	327.7	338.9	44.3%	29.0%

Based on Table 4, the contributions of each factor are analyzed through multi-dimensional comparison.

Impact of the ToU pricing strategy in PV-integrated scenarios (S1 vs. S2): the time-of-use mechanism reduces the total cost by 21.1% (231.2 to 182.5). This underscores that PV energy generation alone is insufficient; it requires price signals to actively schedule storage, "shifting" renewable energy to peak price periods to unlock its temporal value. In contrast, without PV (S3 vs. S4), ToU signals only yield a 6.4% cost reduction via load shifting. The significant disparity in cost reduction validates the necessity of "source-price" coupling, where PV integration amplifies the system's flexibility for peak shaving.

Contribution of PV Configuration: regardless of the pricing strategy, PV integration serves as the primary driver for low-carbon manufacturing. Under both ToU (S1 vs. S3) and flat pricing (S2 vs. S4) conditions, carbon emissions drop significantly from the 340 kg level to the 240 kg level (reductions of 30.5% and 26.8%, respectively). This physical substitution of grid power with clean energy simultaneously lowers operational costs and lowers carbon footprints.

Verification of Synergistic Effect: Scenario 1 achieves global optimality across all metrics, delivering a 44.3% cost reduction and a 29.0% emissions reduction compared to the baseline Scenario 4.

4.5. Algorithm Complexity Analysis

The computational complexity of the proposed algorithm is primarily determined by the iterative process of CMOPSO and the bi-level feedback mechanism. Let N be the population size, G be the maximum number of iterations, D be the encoding dimension (proportional to the total number of operations O_{total}), and M be the number of objectives. The complexity can be analyzed as follows:

Fitness Evaluation: In each iteration, decoding the solution and calculating the objectives (makespan, cost, carbon) requires traversing all operations. The complexity is $O(N \cdot D)$.

Pareto Sorting and Archive Maintenance: The non-dominated sorting (e.g., similar to NSGA-II) typically has a complexity of $O(M \cdot N^2)$.

Bi-level Feedback Loop: Let K be the number of Lagrangian feedback iterations. The entire CMOPSO process is influenced by the weight updates in this outer loop.

Therefore, the overall time complexity of the proposed framework can be approximated as

$$T_{\text{total}} \approx O\left(K \cdot G \cdot \left(N \cdot D + M \cdot N^2\right)\right) \tag{62}$$

Although the introduction of the three-stage strategy and bi-level feedback increases the computational burden compared to single-layer algorithms, it remains within polynomial time complexity. Considering that production scheduling is typically an offline planning task, the priority is solution quality (cost and carbon reduction), rather than millisecond-level real-time response. Empirical results show that the algorithm converges within a reasonable time for standard benchmark instances.

5. Conclusions

This paper proposes a collaborative optimization method for low-carbon scheduling of flexible job shop production considering photovoltaic microgrids that integrates energy allocation and job scheduling after the introduction of photovoltaic energy into the workshop production process and the introduction of a time-sharing tariff policy, with the aim of promoting low-carbon and high-efficiency production activities. Firstly, a PV microgrid, as well as a low-carbon scheduling model, for the flexible workshop are established; secondly, a three-stage problem-solving framework is constructed for the difficulties of the coupled problem of the two- and a multi-objective particle swarm algorithm, which combines chaotic mapping with adaptive mutation mechanism, and is improved for the solving of this model, and a two-tier collaborative optimization architecture is designed based on the CMOPSO algorithm. The final research results are as follows.

(1) The three-stage problem-solving method and the two-layer co-optimization architecture proposed in this paper significantly improve the processing time of shop floor production, as well as the carbon emissions generated in the production process, and a four-layer coding mechanism was designed that conforms to the problem model. The optimization method is tested with the Brandimarte example, and the comparison results show that the optimization method has significant advantages and reliability for this kind of problem.

(2) By exploring the impact of time-sharing tariff policy on low-carbon dispatching of PV flexible workshops and analyzing the interaction between energy allocation and tariffs, the results show that time-sharing tariffs can significantly reduce electricity expenses by increasing the tariffs during peak hours, decreasing the tariffs during low hours, and adjusting the electricity loads to coincide with the peak period of renewable energy generation in order to sub-divide the reduction of the rate of light abandonment.

(3) Simulation verifies the effectiveness of CMOPSO in solving such problems by comparing CMOPSO with three other mainstream multi-objective optimization algorithms (including MOPSO, NSGA-II, and SPEA-II) in a comprehensive manner, which show significant advantages for different kinds of problems and in multiple evaluation dimensions.

This study demonstrates the feasibility of integrating PV microgrids into the valuable flexible job shop scheduling model and verifies the superiority of the optimization framework and algorithms in problem solving. In practical applications, this method can help manufacturing enterprises optimize the scheduling scheme and consider the scheme after the introduction of photovoltaic energy, which can help enterprises improve productivity while effectively reducing carbon emissions and transforming in green and low-carbon directions.

https://doi.org/10.3390/math14040590

Author Contributions: Conceptualization, Q.L. and C.W.; methodology, C.W.; software, C.W.; validation, C.W., Z.G. and X.C.; formal analysis, C.W.; investigation, C.W.; resources, Q.L., C.Z. and G.Z.; data curation, C.W.; writing—original draft preparation, C.W.; writing—review and editing, Q.L., C.W., Z.G., X.C., C.Z. and G.Z.; visualization, C.W.; supervision, Q.L.; project administration, Q.L.; funding acquisition, Q.L. All authors have read and agreed to the published version of the manuscript.

Funding: This work is supported by the National Natural Science Foundation of China (No. 52005400, 52574203); The Natural Science Basic Research Program of Shaanxi Province (2025JC-YBMS-543); and The Scientific Research Program of the Shaanxi Provincial Department of Education–Youth Innovation Team Project (24JP111).

Data Availability Statement: The original contributions presented in this study are included in the article. Further inquiries can be directed to the corresponding author.

Conflicts of Interest: The authors declare no conflicts of interest.

References

1. Tong, Y.; Wang, K.; Liu, J.; Zhang, Y.; Gao, J.; Dan, M.; Yue, T.; Zuo, P.; Zhao, Z. Refined assessment and decomposition analysis of carbon emissions in high-energy intensive industrial sectors in China. *Sci. Total Environ.* **2023**, *872*, 162161. [CrossRef] [PubMed]
2. Tang, Y.; Ding, H.; Shan, X.; Wang, X. Application of the novel three-stage DEA model to evaluate total-factor energy efficiency: A case study based on 30 provinces and 8 comprehensive economic zones of China. *Results Eng.* **2023**, *20*, 101417. [CrossRef]
3. Zhang, Y.; Sun, Z.; Qin, R.; Xiong, H. Idle Duration Prediction for Manufacturing System Using a Gaussian Mixture Model Integrated Neural Network for Energy Efficiency Improvement. *IEEE Trans. Autom. Sci. Eng.* **2019**, *18*, 47–55. [CrossRef]
4. Qu, H.; Tong, X.; Cai, M.; Shi, Y.; Lan, X. Energy-saving scheduling strategy for variable-speed flexible job-shop problem considering operation-dependent energy consumption. *Expert Syst. Appl.* **2024**, *256*, 124952. [CrossRef]
5. Savchenko, M.; Radchuk, O.; Gerasimenko, V.; Chepizhnyi, A. Development of a methodology for calculating the consumption of a combined renewable energy source for a mini–workshop. *IOP Conf. Ser. Earth Environ. Sci.* **2024**, *1429*, 012018. [CrossRef]
6. Guo, J.; Luo, Q.; Liang, P.; Ouyang, J. A GAPN Approach for the Flexible Job-Shop Scheduling Problem with Indirect Energy and Time-of-Use Electricity Pricing. *Processes* **2022**, *10*, 832. [CrossRef]
7. Zhao, Z.; Zhou, M.; Liu, S. Iterated Greedy Algorithms for Flow-Shop Scheduling Problems: A Tutorial. *IEEE Trans. Autom. Sci. Eng.* **2022**, *19*, 1941–1959. [CrossRef]
8. Zhang, X.; Liu, S.; Zhao, Z.; Yang, S. A Decomposition-Based Evolutionary Algorithm With Clustering and Hierarchical Estimation for Multi-Objective Fuzzy Flexible Jobshop Scheduling. *IEEE Trans. Evol. Comput.* **2024**, *30*, 2–15. [CrossRef]
9. Zhang, X.; Zhao, Z.; Qin, S.; Liu, S.; Zhou, M. Dynamic quadratic decomposition-based evolutionary algorithm for multi-objective fuzzy flexible jobshop scheduling. *Swarm Evol. Comput.* **2025**, *94*, 101884. [CrossRef]
10. Luan, F.; Zhao, H.; Liu, S.Q.; He, Y.; Tang, B. Enhanced NSGA-II for multi-objective energy-saving flexible job shop scheduling. *Sustain. Comput. Inform. Syst.* **2023**, *39*, 100901. [CrossRef]
11. Liu, M.; Lv, J.; Du, S.; Deng, Y.; Shen, X.; Zhou, Y. Multi-resource constrained flexible job shop scheduling problem with fixture-pallet combinatorial optimisation. *J. Comput. Ind. Eng.* **2024**, *188*, 109903. [CrossRef]
12. Meng, L.; Zhang, C.; Shao, X.; Ren, Y. MILP models for energy-aware flexible job shop scheduling problem. *J. Clean. Prod.* **2019**, *210*, 710–723. [CrossRef]
13. Wei, Z.; Liao, W.; Zhang, L. Hybrid energy-efficient scheduling measures for flexible job-shop problem with variable machining speeds. *Expert Syst. Appl.* **2022**, *197*, 116785. [CrossRef]
14. Luo, C.; Gong, W.; Lu, C. Knowledge-driven two-stage memetic algorithm for energy-efficient flexible job shop scheduling with machine breakdowns. *Expert Syst. Appl.* **2024**, *235*, 121149. [CrossRef]
15. Du, Y.; Li, J.; Li, C.; Duan, P. A Reinforcement Learning Approach for Flexible Job Shop Scheduling Problem With Crane Transportation and Setup Times. *IEEE Trans. Neural Netw. Learn. Syst.* **2022**, *35*, 5695–5709. [CrossRef]
16. Lv, Y.; Li, C.; Tang, Y.; Kou, Y. Toward Energy-Efficient Rescheduling Decision Mechanisms for Flexible Job Shop With Dynamic Events and Alternative Process Plans. *IEEE Trans. Autom. Sci. Eng.* **2022**, *19*, 3259–3275. [CrossRef]
17. Zhao, Z.; Li, X.; Liu, S.; Zhou, M.; Yang, X. Multi-Mobile-Robot Transport and Production Integrated System Optimization. *IEEE Trans. Autom. Sci. Eng.* **2025**, *22*, 7480–7491. [CrossRef]
18. Chen, W.; Fujii, M.; Sun, L. Feasibility analysis of energy system optimization for a typical manufacturing factory with environmental and economic assessments. *J. Clean. Prod.* **2022**, *366*, 132887. [CrossRef]
19. Chakraborty, S.; Arvind, P.; Kumar, D. Coordinated Control for Frequency Regulation in a Stand-Alone Microgrid Bolstering Demand Side Management Capability. *Electr. Power Compon. Syst.* **2021**, *49*, 1–17. [CrossRef]

20. Huang, C.; Zhang, H.; Song, Y.; Wang, L.; Ahmad, T.; Luo, X. Demand Response for Industrial Micro-Grid Considering Photovoltaic Power Uncertainty and Battery Operational Cost. *IEEE Trans. Smart Grid* **2021**, *12*, 3043–3055. [CrossRef]
21. Zhang, R.; Li, G.; Jiang, T.; Chen, H.; Li, X.; Pei, W.; Xiao, H. Incorporating Production Task Scheduling in Energy Management of an Industrial Microgrid: A Regret-Based Stochastic Programming Approach. *IEEE Trans. Power Syst.* **2021**, *36*, 2663–2673. [CrossRef]
22. Burmeister, S.C.; Guericke, D.; Schryen, G. A two-level approach for multi-objective flexible job shop scheduling and energy procurement. *Clean. Energy Syst.* **2025**, *10*, 100178. [CrossRef]
23. Li, D.; Li, Z.; Li, X.; Yu, J.; Yang, M.; Lei, X. Optimization method of time-of-use electricity price for the cost savings of power grid investment. *Front. Energy Res.* **2024**, *12*, 1361116. [CrossRef]
24. Yu, G.; Cheng, B.; Xu, T.; Pan, J.; Chen, Y. Multi-level task network scheduling and electricity supply collaborative optimization under time-of-use electricity pricing. *Comput. Ind. Eng.* **2025**, *203*, 110952. [CrossRef]
25. Jia, S.; Yang, Y.; Li, S.; Wang, S.; Li, A.; Cai, W.; Liu, Y.; Hao, J.; Hu, L. The Green Flexible Job-Shop Scheduling Problem Considering Cost, Carbon Emissions, and Customer Satisfaction under Time-of-Use Electricity Pricing. *Sustainability* **2024**, *16*, 2443. [CrossRef]
26. Park, M.-J.; Ham, A. Energy-aware flexible job shop scheduling under time-of-use pricing. *Int. J. Prod. Econ.* **2022**, *248*, 108507. [CrossRef]
27. Shen, L.; Dauzère-Pérès, S.; Maecker, S. Energy cost efficient scheduling in flexible job-shop manufacturing systems. *Eur. J. Oper. Res.* **2023**, *310*, 992–1016. [CrossRef]
28. Shui, J.; Peng, D.; Song, Y.; Zhou, Q. Optimal scheduling strategy of virtual power plant with carbon emission and carbon penalty considering uncertainty of wind power and photovoltaic power. *J. Syst. Simul.* **2024**, *36*, 305–319. [CrossRef]
29. Wu, X.; Shan, Y.; Fan, K. A Modified Particle Swarm Algorithm for the Multi-Objective Optimization of Wind/Photovoltaic/Diesel/Storage Microgrids. *Sustainability* **2024**, *16*, 1065. [CrossRef]
30. Yan, J.; Wang, C. Stamping workshop scheduling optimization considering multiple constraints under time-of-use electricity pricing. *Comput. Ind. Eng.* **2025**, *206*, 111199. [CrossRef]
31. Wang, D.; Tan, D.; Liu, L. Particle swarm optimization algorithm: An overview. *Soft Comput.* **2018**, *22*, 387–408. [CrossRef]
32. Zhang, Q.; Hu, J.; Liu, Z.; Duan, J. Multi-objective optimization of dual resource integrated scheduling problem of production equipment and RGVs considering conflict-free routing. *PLoS ONE* **2024**, *19*, e0297139. [CrossRef]
33. Brandimarte, P. Routing and scheduling in a flexible job shop by tabu search. *Ann. Oper. Res.* **1993**, *41*, 157–183. [CrossRef]
34. Ma, H.; Zhang, Y.; Sun, S.; Liu, T.; Shan, Y. A comprehensive survey on NSGA-II for multi-objective optimization and applications. *Artif. Intell. Rev.* **2023**, *56*, 15217–15270. [CrossRef]
35. Zou, Y.; Huang, H.; Xia, X.; Wang, X.; Quaranta, G. Design Optimization of Curved Curtain Wall Based on SPEA II-GA-BPNN Algorithm. *Adv. Civil. Eng.* **2022**, *2022*, 2548647. [CrossRef]
36. Cui, H.; Zhang, H.; Zhou, L.; Yang, C.; Li, B.; Zhao, X. Fuzzy analytic hierarchy process with ordered pair of normalized real numbers. *Soft Comput.* **2023**, *27*, 12267–12288. [CrossRef]
37. Lu, Q.; Chen, Y.; Zhang, X. Grinding process optimization considering carbon emissions, cost and time based on an improved dung beetle algorithm. *Comput. Ind. Eng.* **2024**, *197*, 110600. [CrossRef]

Disclaimer/Publisher's Note: The statements, opinions and data contained in all publications are solely those of the individual author(s) and contributor(s) and not of MDPI and/or the editor(s). MDPI and/or the editor(s) disclaim responsibility for any injury to people or property resulting from any ideas, methods, instructions or products referred to in the content.